学位論文

Optical Control of Neurite Outgrowth Direction in Living Organisms with Light-Induced Protein Oligomerization System

（タンパク質光多量体形成反応を用いた

生体内における神経軸索伸長方向の制御の確立）

平成２７年１２月　博士（理学）申請

東京大学大学院理学系研究科化学専攻

Mizuki Endo

遠藤 瑞己

Abstract

Precise construction of neural circuits requires tightly controlled wiring of individual axons during nervous system development. Growth cones of extending axons navigate to correct targets by sensing a guidance cue gradient via membrane protein receptors. Moreover, the axonal wiring is further modified in living organisms by highly complicated environments with heterogeneous extracellular matrix and structures. Although most signaling mechanisms regarding to the ligand–receptor reactions have been intensively investigated by an *in vitro* approach, due to the lack of tools, it is still difficult to examine the modulation of growth cone behavior by the extracellular environment in living animals (**Chapter 1**).

Herein, in the present thesis, I developed an optical system that has a potential to control the direction of axonal outgrowth by activating the axon guidance receptor protein, Deleted in Colorectal Cancer (DCC). In the physiological condition, cytoplasmic domain of DCC oligomerizes upon its extracellular ligand binding, which is important for activating the intracellular signaling for cytoskeletal remodeling. To regulate the oligomerization by external light, light-inducible clustering module of the flowering plant *Arabidopsis thaliana* photoreceptor Cryptochrome2 (CRY2) was genetically connected with DCC, named photo-activatable DCC (PA-DCC). Blue-light illumination transiently activates DCC by oligomerization, which triggers downstream signaling in the illuminated subcellular region. The extending axons were attracted by illumination in cultured chick dorsal root ganglion neurons (**Chapter 3**).

Moreover, I established a transgenic nematode worm *Caenorhabditis elegans* expressing the axonal light-induced attraction system using the homolog of PA-DCC. The light-mediated navigation of the developing growth cones was achieved in living *C. elegans*. The photo-manipulation system was also applied to investigate the relationship between the growth cone

behavior and its surrounding environment in living tissue. From the analysis, the restriction of the growth cone motility by the extracellular structures was confirmed (**Chapter 4**).

Materials and experimental details are described in **Chapter 2**. Final conclusion of this thesis is given in **Chapter 5**.

Chapter 1.

General Introduction

1.1 Introduction of axon guidance

1.1.1. Development of the nervous system

The nervous systems in adult human consist of more than 1×100 billion neurons, where each neuron is connected with about 10,000 other neurons[1, 2]. Neurons do not only localized to the brain, but spread throughout the body. The nervous system can be divided into two parts: central nervous system (CNS) and the peripheral nervous system (PNS)[3]. The CNS contains brain and spinal cords, where the information from the body are integrated and processed. The PNS is composed of neurons and neuronal cell cluster, called ganglia, outside of the CNS. The main role of PNS is to connect CNS with "peripheral" tissues, including limbs and organs, mediating the communication of the information between CNS and those tissues. Although each system is derived from the different ectoderms, neural tube for CNS or neural crest for PNS, both cell progenitors are specified into the same specific cell type as a neuron[4, 5].

Neuron has a distinct morphological character, which is specialized for network formation (**Figure 1-1a**). Dendrites are the fine, branching structures protruded from the cell body. They receive electric impulses from other cells via connections called synapses, and transmit them to the cell body. Whereas dendrites do not extend far from the cell body, a neurite called axon may extend about 1 meter[6]. Once the electric impulses gathered at the cell body exceed the threshold of electric potential, an action potential generated from the cell body propagates through the axon and transmits the electric impulses from the tip to other cells via synapses. By repeating these events among neurons, neural network processes the electric information via a numerous synaptic connections to achieve complicated motor or cognitive functions. Because the information processing within neural network entirely depends on the neuronal connectivity, precise axonal wiring is crucial for the nervous development.

During the formation of neural network, neurons extend axons to find their correct synaptic targets. At the tip of axons, there is a motile, palm-like structure called growth cone (**Figure 1-1b**). Based on the morphology, the growth cone is divided into three regions: central domain, transitional zone, and peripheral domain[7]. The central domain is located at the center of the growth cone nearest to the axon, where a dense microtubule bundles extend from the axon. Because of the bundles, the area of the central domain can be defined by the upheaval region in the growth cone. In contrast to the central domain, the peripheral domain is a thin region surrounding the edge of the growth cone. The peripheral domain is mainly composed of actin-based structures. Filopodia is a finger-like structure composed of F-actin bundles, which continuously repeats protrusion and contraction around the edge. It is followed by ruffling webbing-like structure called lamellipodia, which contains a dense F-actin network. The continuous polymerization and depolymerization of actin enables the dynamic rearrangements of these structures. The transition zone is an interface region between the central and the peripheral domain. By the dynamic movements of the peripheral domain, growth cones continuously seek and sense the extracellular guidance cue molecules. Guided by these molecules, growth cones move toward their targets, followed by their axonal extension with microtubule elongation.

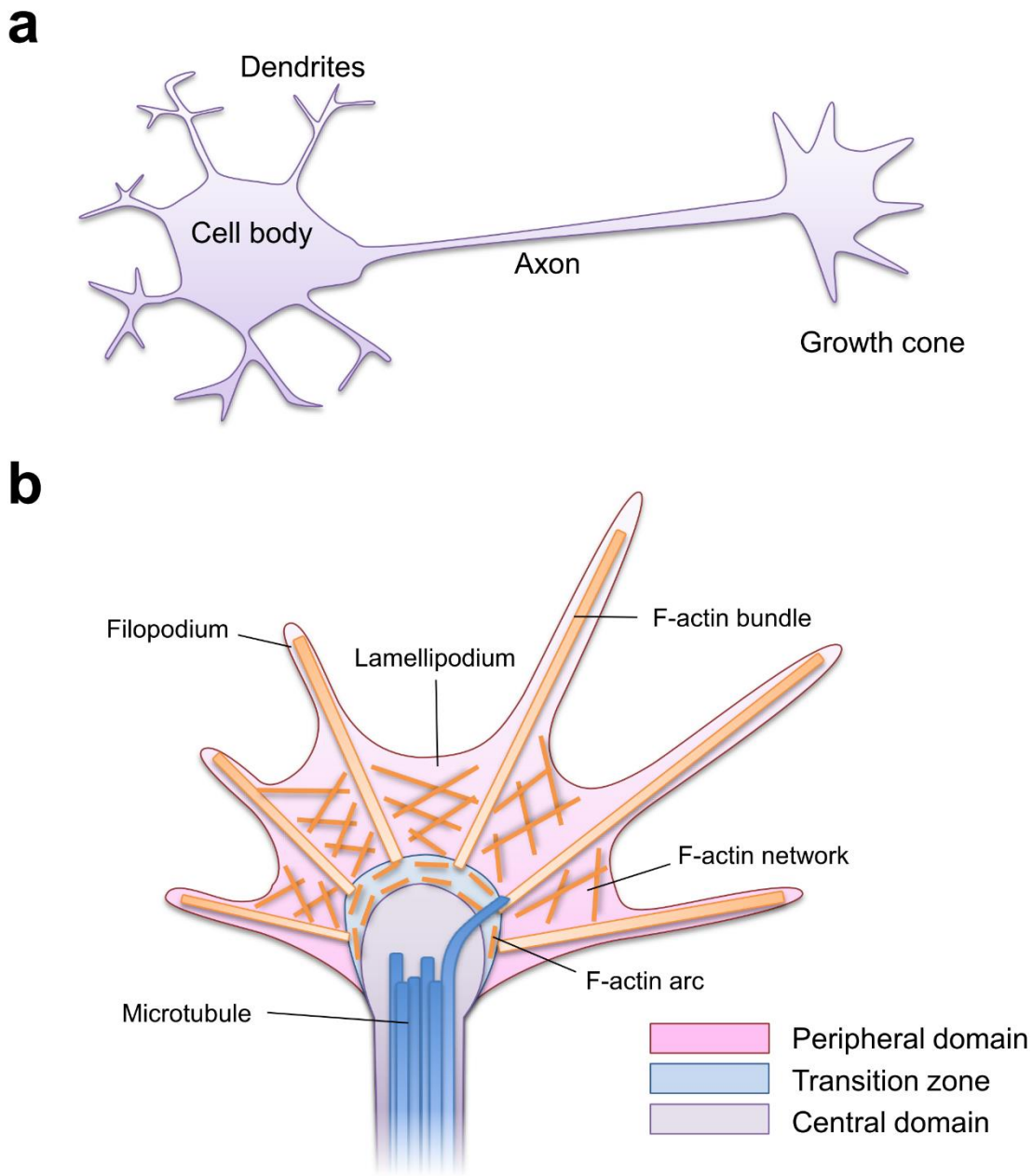

Figure 1-1. Structures of the neuron and the growth cone.

(**a**) Structure of the neuron. (**b**) Structure of the growth cone. Each domain was shown by each represented color.

1.1.2. Mechanisms of axon guidance

Growth cones respond to the extracellular guidance cue proteins, attractant or repellant[8]. These molecules are secreted by surrounding cells and generate its gradients by a long-range diffusion. Because growth cones express specific receptors for them on plasma membrane, they are able to recognize cues to determine the orientation of axonal outgrowth.

There are several axon guidance molecule families which highly conserved in various species: netrins, slits, ephrins, and semaphorins (**Figure 1-2a**)[9]. Each guidance molecule has corresponded binding receptors: Eph for ephrins, Deleted in Colorectal Cancer (DCC) and UNC-5 for netrins, Plexin and Neuropilin for semaphorins, and Robo for slits. Upon ligands binding, the receptors are activated by conformational change or by simple oligomerization. For example, whereas Plexin forms activated dimer by the conformational change upon semaphorin binding[10], DCC is thought to be activated simply by netrin-1-mediated bridging[11]. Moreover, different receptors sometimes interact with each other to modify the responses: Robo is able to interact with DCC to inhibit netrin-1/DCC mediated attractive response during midline crossing of commissural axons[12]. To generate a variety of circuits in nervous system in developing embryos, these guidance molecules and receptors cooperate with each other[13].

The regulation of cytoskeleton structures is one of the key roles in the reaction of axon guidance receptors. The activated receptors control the activity of the Rho family GTPases, RhoA, Rac1, and Cdc42 via GTPase-activating proteins (GAPs) or guanine nucleotide exchange factors (GEFs) (**Figure 1-2b**)[14]. The Rho GTPases subsequently activates various cytoskeletal effectors, including ROCK, Enabled, and ARP2/3. These effectors induce assembly or disassembly of F-actin, thereby controlling the protrusion or contraction of filopodia and lamellipodia. Microtubules are also regulated in a similar way. While attractive ligand–receptor reactions

stabilize and lengthening the cytoskeletal structures, repulsive reaction destabilize and shorten them.

The modulation of the cell adhesion is another important step for the growth cone movements[15]. During the directional movement of the growth cone, adhesion complexes, called focal contacts, provide clutches for the contractile machinery composed of actin and motor proteins, myosin. Among a number of focal contact components, focal adhesion kinase (FAK) plays a crucial role in the assembly and the degradation of focal contacts[16]. In attractive signaling such as netrin-1/DCC pathway, for instance, FAK is activated in response to the netrin-1 gradient and mediates mechanical forces by myosin II, a motor protein[17]. Although detailed mechanisms are yet to be clarified, coordination of the cell adhesion modulation and the cytoskeletal remodeling seems to be critical for the directional movements of the growth cones.

Moreover, growth cone movements are also influenced such as membrane turn over[18], Ca^{2+} signaling[19], and the concentration of cyclic adenosine monophosphate (cAMP)[20] and cyclic guanosine monophosphate (cGMP)[21]. By integrating all the biomolecular signaling described above, growth cones constantly decide the orientation of the axonal outgrowth in the axonal navigation during the nervous development.

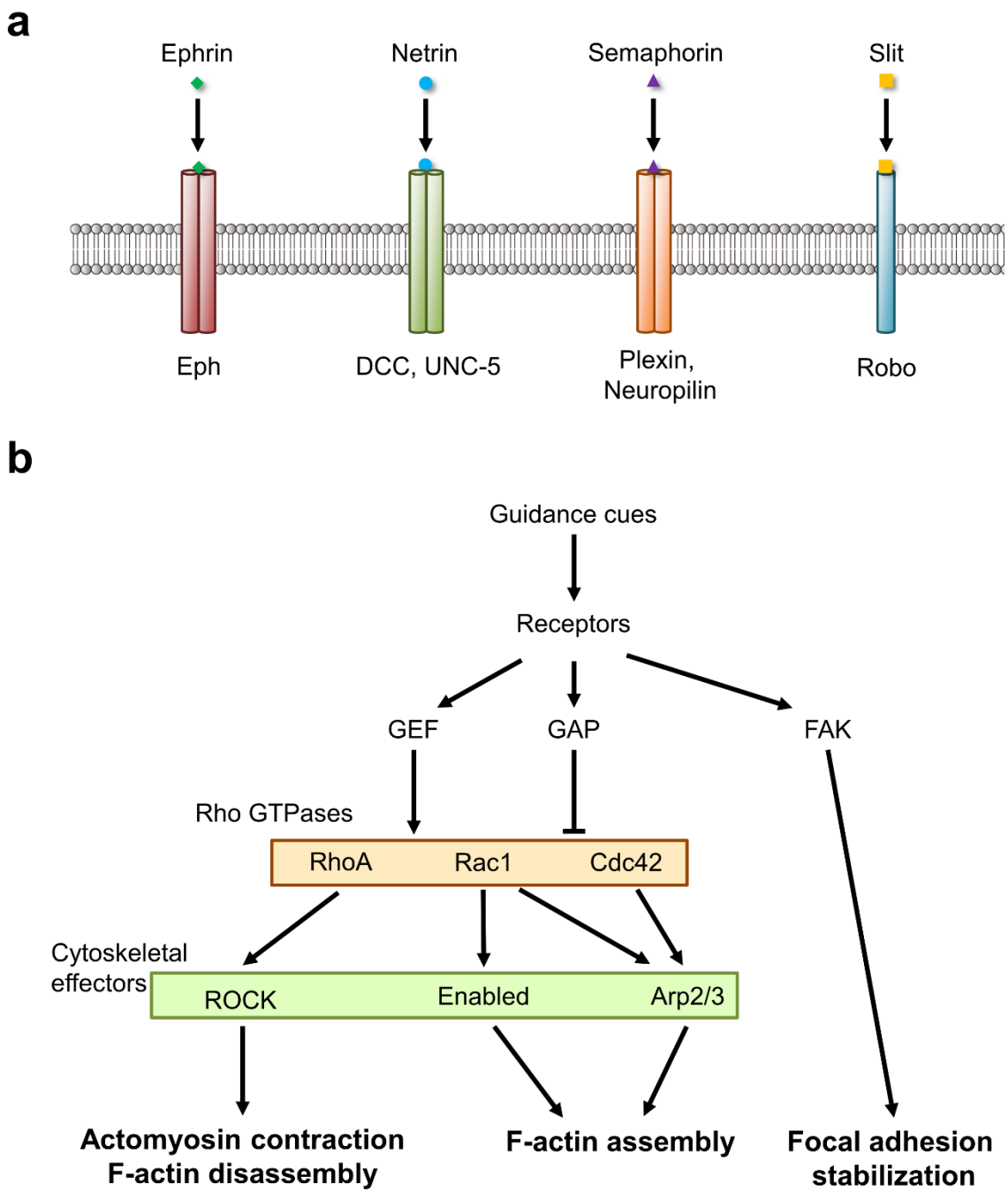

Figure 1-2. Mechanisms of axon guidance.

(**a**) Four major ligand–receptor pairs in axon guidance. (**b**) Molecular signaling of axon guidance for cytoskeletal remodeling and cell adhesion modulation. Arrows indicate activation, whereas T-bars indicate suppression.

1.1.3. Modulation of axon guidance by extracellular environments

The axonal navigation by guidance cue molecules is further modulated in living tissue. The extracellular matrix, which normally serves as a scaffold for the extending axons, is able to modulate intracellular guidance signaling. For instance, laminin-1, an extracellular matrix component, induce nitric oxide (NO) production by NO synthase in the cytoplasm (**Figure 1-3**)[22]. Subsequently, NO increases intracellular cGMP levels by activating guanylyl cyclase. Then, the increased cGMP level affects various protein activities through protein kinase G activation which typically leads to the conversion of the guidance signaling in several pathways[23, 24]. Similarly, the cAMP level is also regulated by another extracellular substrate such as L1, which generally promotes attractive signaling. As described above, the modulation of cAMP/cGMP ratio by extracellular matrix affects the output of axon guidance signaling pathway[23].

The extracellular structures also modulate the direction of neurite outgrowth by physical barriers or cellular adhesions. In the nervous system, CNS and PNS are strictly separated except for motor neurons, which innervate muscles in the body and transmit electric impulses from CNS. The integrity of the CNS is achieved by a basal lamina coat composed of extracellular matrix surrounding the spinal cord[25]. Motor neurons, by contrast, are able to exit from the spinal cord form the gaps occurred in the barriers. Another example of the modulation is “pioneer neurons”. While an embryo is small and tissue arrangement is simple, pioneer neurons migrate to their targets. Later in the development, other neurons adhere to them and form nerve bundle, where attached neurons extend along the direction of the pioneer axons. The nerve bundles also affect other growth cone motility and orientation of axonal elongations[26, 27]. Therefore, the heterogeneous extracellular environments affect the guidance-cue-mediated axon guidance, which is essential for the highly complicated neural wirings during the nervous development.

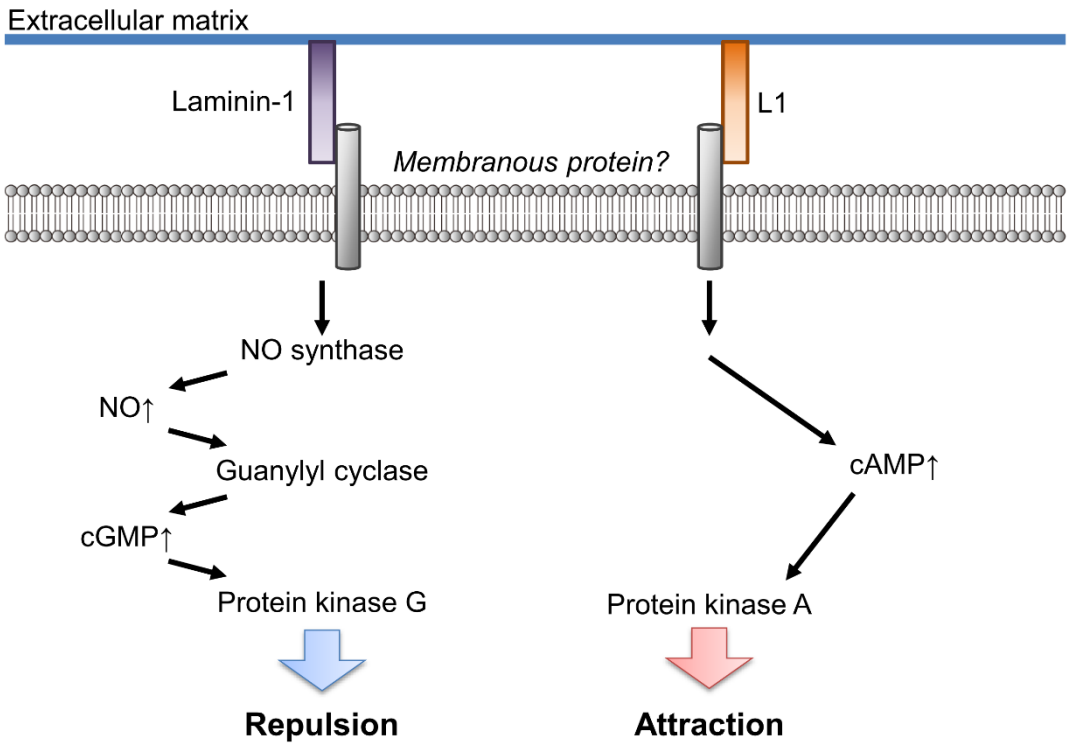

Figure 1-3. Modulation of axon guidance signaling by extracellular matrix substrates. Arrows indicate activation.

1.1.4. *In vitro* analysis of axon guidance mechanisms

The mechanisms of axon guidance have been intensively analyzed in *in vitro* experiments with cultured neurons. One of the historically important experiment is co-culture assay[28]. In this assay, a neuronal tissue such as ganglia is taken from the developing nervous system and co-cultured with target tissue explants in collagen gels. If the target cells secretes attractant, the neuronal tissue extends axons toward the target, while extends axons away from the target if it secretes repellant. With the advances in the genetic techniques, a modified version was also invented using transfected cells secreting the candidate targets[29]. A number of guidance cue molecules have been identified and investigated with the co-culture assay[29-34].

The growth cone turning assay is another important experimental system that has been contributed to the understanding of the underlying mechanisms in ligand-induced axon guidance signaling[21]. In this assay, a reproducible chemical gradient of a certain molecule is generated ahead of extending axons by a pulse application from a pipette. Chemical compounds, including cyclic nucleotide analogs[21] and modulators for specific signaling pathways[18, 35], have been used to unveil the signaling mechanisms of the systems. In addition to the methods described above, fluorescent imaging of second messenger concentrations or protein activities also substantially contributed to the investigation of the signaling pathways[36-39].

Although most of the axon guidance mechanisms have been clarified by these techniques, the roles of the other important factors, modulations by extracellular environment in living tissues, are not fully understood because of the lack of tools. Because the environments surrounding the developing axons are heterogeneous and continuously changing, a novel method to analyze the guidance signaling with intact organisms is required.

Recently, optogenetics, which is a system that optically control the protein activities to modulate cellular behavior, has been attracting a wide attention[40, 41]. It is because of its ability to achieve high spatiotemporal resolution in living organisms[42-44]. Besides its applicability to *in vivo* experiments, another advantage of the optical stimulation is that it allows easy modulation of the protein activation level with the light intensity or duration[45-47]. Accordingly, optical regulation of the axon guidance signaling *in vivo* has a potential to analyze the interplay between developing axons and surrounding heterogeneous environments.

1.2 Regenerative therapy for the diseased neural circuits

1.2.1. Impaired axonal wiring in diseased nervous system

In developing embryos, the axon guidance systems described in the previous sections dynamically coordinated with each other to generate a variety of circuits in nervous system. However, especially in CNS, these dynamic regulations of axon guidance for neural circuit generation are limited only at embryonic stages[48]. Therefore, neural disconnection among functional neuron groups in CNS caused by neurodegenerative disorders or brain injury typically leads to persistent neurological deficits because of the inability to regrow axons spontaneously.

Basal ganglia is a key area within CNS located deep in the brain, which is indispensable for the regulation of the motor movements[49]. The basal ganglia mediates neuronal connection between cerebral cortex and thalamus, comprising a motor loop (**Figure 1-4a**). Within the basal ganglia, there are several important neuronal groups. Among them, striatum receives information inputs from cerebral cortex and modulates the thalamic activation of cerebral motor cortex via two pathway: direct pathway and indirect pathway. Whereas the direct pathway promotes movements by activation of the thalamus, the indirect pathway inhibits by inactivation. The dysfunction of the components in the basal ganglia disrupts the balance between the pathways, resulting in hyperkinetic or hypokinetic symptoms[50].

In patients with Huntington's disease, neurons in the striatum are degenerated (**Figure 1-4b**). The degeneration severely impairs the indirect pathway and leads to excessive stimulation of cerebral cortex by the thalamus, resulting in hyperkinetic including chorea. In another example, Parkinson's disease, dopaminergic neurons in the regulatory component for striatum is degenerated (**Figure 1-4c**). Their loss constitutively inactivates the direct pathway and activates the indirect pathway, therefore patients with Parkinson's disease exhibit hypokinetic symptoms

like akinesia. Because mature neurons lack the ability to regenerate, these deficits persist almost permanently. For this reason, there is a great interest in the possibility of reconnecting the nervous system.

Cell replacement therapy is one of the promising methods for the regeneration of the diseased or damaged nervous system[51, 52]. In this therapy, immature neural precursors are implanted into the host brain, allowing them to restore functional connection with appropriate targets. There is already much evidence from animal experiments showing that the neural stem cell transplantation results in recovery of neural function. Furthermore, some clinical trials to human patients have yielded proof-of-principle that cell transplantation restored synaptic connections to some extent in Parkinson's disease patients[53]. Recently, induced pluripotent stem cells are expected as a source of neural precursors because they enable to overcome immunological rejection or ethical concerns[54].

Although cell replacement therapy has a great potential for reconstitution of neural circuits in CNS, the formation of spontaneous appropriate neural connections is sometimes inefficient. Moreover, it is extremely challenging for the replacement therapy to cure diffuse disorders such as Alzheimer's disease or stroke, where multiple neuronal subtypes and groups are damaged, because of the grafts' rare re-innervations to their correct targets[55]. The inefficient and inappropriate connectivity is in danger of diminishing the therapeutic efficacy and, moreover, deteriorating symptoms. Consequently, controlling the axonal projection of implanted neurons is indispensable for clinical application.

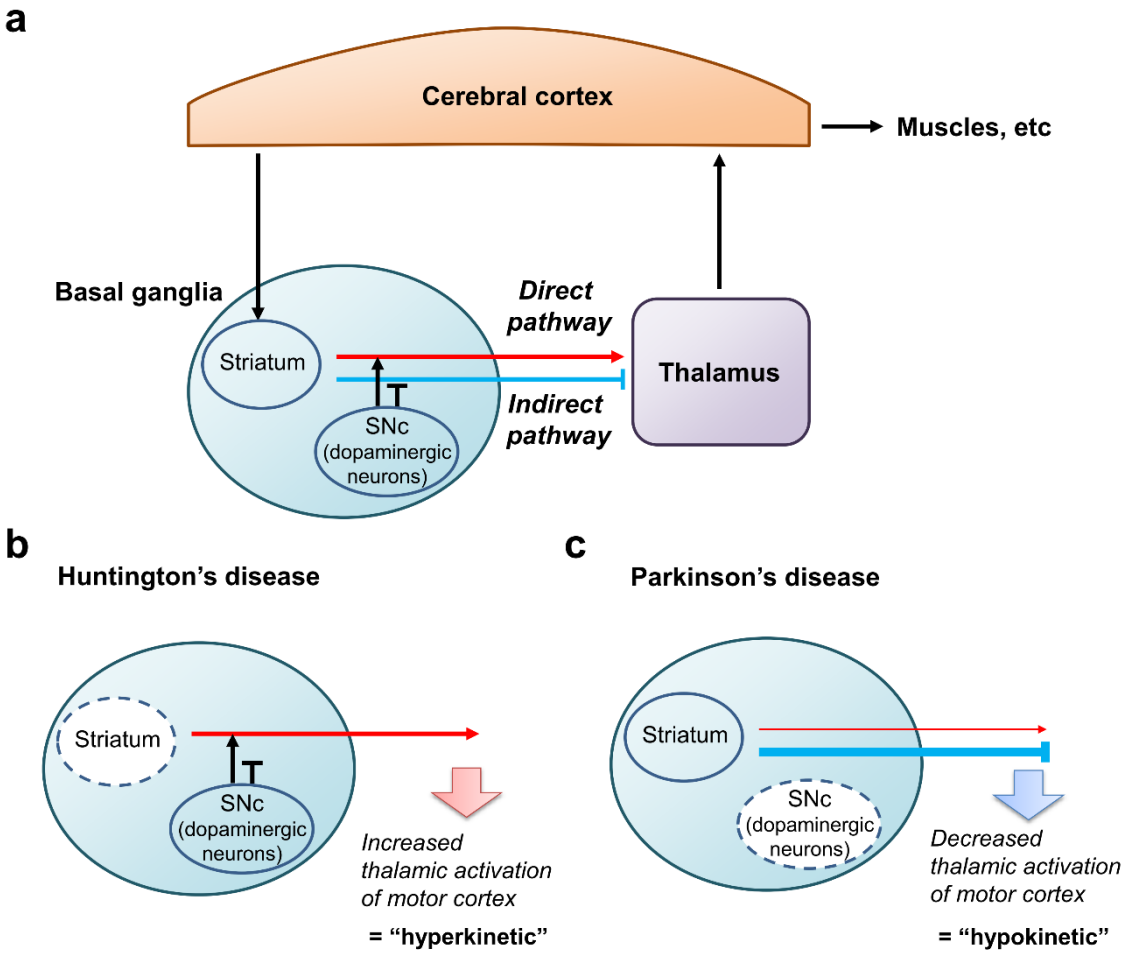

Figure 1-4. Neurodegeneration in basal ganglia.

(**a**) Neural network of the motor loop among cerebral cortex, basal ganglia, and thalamus. Arrows indicate activation, whereas T-bars indicate suppression. SNc represents substantia nigra compacta, a regulatory component of striatum in basal ganglia. (**b**) Neurodegeneration in striatum in Huntington's disease. Dashed circles indicate neuronal degeneration areas. (**c**) Neurodegeneration in SNc in Parkinson's disease.

1.2.2. Controlling the orientation of neurite outgrowth

Up to now, various technologies for regulating axon pathfinding have been developed. Local administration of guidance cues is the most classical methods for inducing growth cone steering[21]. Although this technique is widely adopted for growth cone turning assay, guidance molecule is highly diffusible, thereby reducing precision in steering angle[56]. In contrast, engineered cell culturing systems have achieved high spatial resolution. They are based on the modulation of local cellular adhesiveness with surface fabrication, and patterned guidance cue distribution with microfluidics or microcontact printing[57]. Three dimensional biomaterials such as hydrogel matrix also elicited neurite outgrowth response[58]. These techniques have provided profound insight into the mechanisms of axon guidance, however, they are only applicable to *in vitro* experiments.

The ideal method for axon guidance regulation in regenerative therapies for nervous disorders is to control the activity of proteins involved in the guidance such as receptors with high spatiotemporal precision *in vivo*. Compared to regulating guidance cues, regulating receptors is capable of eliciting attractive or repulsive response only in the target axon. One of the promising approach for fulfilling the requirements is “optogenetics”, as mentioned in the previous sections. The optical control of the neurite outgrowth direction by activating the guidance receptors, has a potential to achieve artificial wiring of the implanted neurons in the replacement therapy. Together with the need in basic science mentioned in the previous sections, development of the optical regulation system that enables photo-activation of the guidance receptors in living organisms, is required.

1.3 Optical control of the protein activity with photoreceptor proteins

1.3.1. Introduction of optogenetics

Optogenetics refers to the integration of optics and genetics, which uses genetically encoded systems that regulate the activity of specific proteins with external light. The optogenetic systems enable the optical perturbation of various biological events in specific cells both *in vitro* and *in vivo*. Recently, various genetically-encoded optogenetic tools were generated to control gene expression[59], ion flux[60], production of second messengers[42], and kinase activities[61] . These technologies have experimental advantages, such as high spatiotemporal precision and *in vivo* availability[42-44]. These advantages broadly expanded the variety of experiments.

Typical optogenetic tools require light-sensitive proteins known as photoreceptor proteins, mainly derived from microbes or plants[62, 63]. Each photoreceptor absorbs its specific wavelength light, ranging from ultraviolet (UV) to near infrared (IR), and triggers biological responses such as visual perception, phototaxis, and flowerings. All photoreceptors possess light-absorbing unit called chromophores, which are mostly organic compounds incorporated into the internal pocket of the protein during the folding. Photon in the spectrum captured by their conjugated pi-bond system excites an electron from its ground state to an excited state. Subsequently it leads to a variety of chemical reactions, including isomerization, electron transfer, and formation of a covalent bond. These processes affect atomic location and electron distribution of the chromophore, which affect the arrangement of the surrounding amino acids chains. The changes around the chromophore propagate throughout the photoreceptor, leading to the overall conformational changes. Finally, the photo-converted photoreceptor exerts function, simply by the conformational changes itself such as channel opening, or by the interactions with other proteins.

Up to now, photoreceptors themselves or fusion proteins with targets were introduced into cells as optogenetic tools to control various biological phenomena. The tools can be divided into two groups based on the characters: conformational change-based and interaction-based. The former group includes light-gated ion channels[60]. These proteins such as Channelrhodopsin2 open their ion channels upon light absorption, which enables optical activation or inactivation of a specific neuron with high spatiotemporal precision in living animals. Recently, numerous light-gated ion channel variants were generated to control neural activity with different kinetics and wavelength, which have been greatly contributed to the neuroscience research field[64]. The latter group has exploited photoreceptors as light-induced interaction modules to trigger various biological signaling mainly by forced protein-protein interactions[65]. In this system, photoreceptor protein and its interacting partner were fused with target proteins, respectively, result in biological signaling. Light-induced homo-oligomerization of photoreceptors were also used to activate proteins[66-71].

Both approaches, conformational change-based and interaction-based, have tremendous potential for the development of the optical systems to control various protein activities. Each strategy has its suitable series of photoreceptors. Because several families of axon guidance receptors require their oligomerization for the activation, photoreceptors called cryptochrome, which is used in the latter interaction-based approach, will be focused in the following section.

1.3.2. Photoreceptor protein cryptochrome 2 from *Arabidopsis thaliana*

The photolyase/cryptochrome family is composed of blue light (400–500 nm) absorbing flavoproteins, proteins containing a nucleic acid derivative of riboflavin[72]. Photolyase is a DNA repair enzyme activated by blue light. It repairs UV-induced DNA damages such as pyrimidine dimers, which sometimes inhibit replication or transcription. Cryptochrome has no photolyase activity, but acts as a key light-dependent component in various biological events including circadian rhythms, plant development, and magnetoreceptions. Both proteins have photolyase homology region (PHR) domain, a highly conserved domain that contains a flavin adenine dinucleotide (FAD) as a chromophore. Among the photolyase/cryptochrome family, cryptochrome 2 (CRY2) from flowering plant *Arabidopsis thaliana* is widely used for the development of the optogenetic tools[47, 66-68, 70, 73-76].

The chromophore FAD undergoes various chemical reactions upon blue light absorption in the photolyase/cryptochrome family. Regarding *Arabidopsis thaliana* CRY2, however, a detailed mechanisms of the light-induced reactions in FAD are still controversial (**Figure 1-5**)[77]. In one proposed model, CRY2 has oxidized FAD in the dark state. By electron transfer, the oxidized FAD is reduced to different forms depending on the wavelength: the neutral semiquinone radical FADH• with blue light, and hydroquinone $FADH^-$ or protonated hydroquinone $FADH_2$ with green light. Among the reduced form of FAD, the neutral semiquinone radical FADH• causes conformational change in CRY2. This model is consistent with several experimental observations. However, alternative model still argues that the deprotonated anionic radical $FAD^{\bullet -}$ is responsible for the photo-conversion of CRY2. Whichever semi-reduced form the chromophore FAD takes upon light absorption, the semi-reduced FAD is gradually oxidized to the original state in dark condition.

In plant cells, photo-converted CRY2 interacts with various proteins, including CIB1, COP1, and SPA[78]. CRY2s also interact with themselves in a light-dependent manner. Subsequently, the CRY2 complex grows to a visible aggregation called photobody in nucleus. Through these interactions CRY2 modulates flowerings, root growth[79] and phototropism[80]. For instance, In CRY2-CIB1 pathway, the CRY2-interaction activates the transcription factor CIB1, which positively regulates the transcription of flowering genes.

Because the CRY2's chromophore FAD is present in mammalian cells, the photoreceptor CRY2 is readily applicable for the development of optogenetic tools. In the previously reported optogenetic systems, CRY2 is used as light-induced protein-protein interaction module, either for hetero-dimerization or for homo-oligomerization. In light-induced hetero-dimerization system, CRY2-CIB1 pair was used for the forced protein-protein interaction to modulate gene expression or epigenetic states[73]. Membrane anchoring of CIB1 also enabled the recruitment of CRY2-fused target proteins, which is activated on cell membrane. In homo-oligomerization system, PHR domain of CRY2 was fused with various proteins, including transmembrane receptor proteins, to activate with external light[66-68, 70, 71]. Both systems achieved rapid interaction in millisecond scale, and gradual dissociation within minutes.

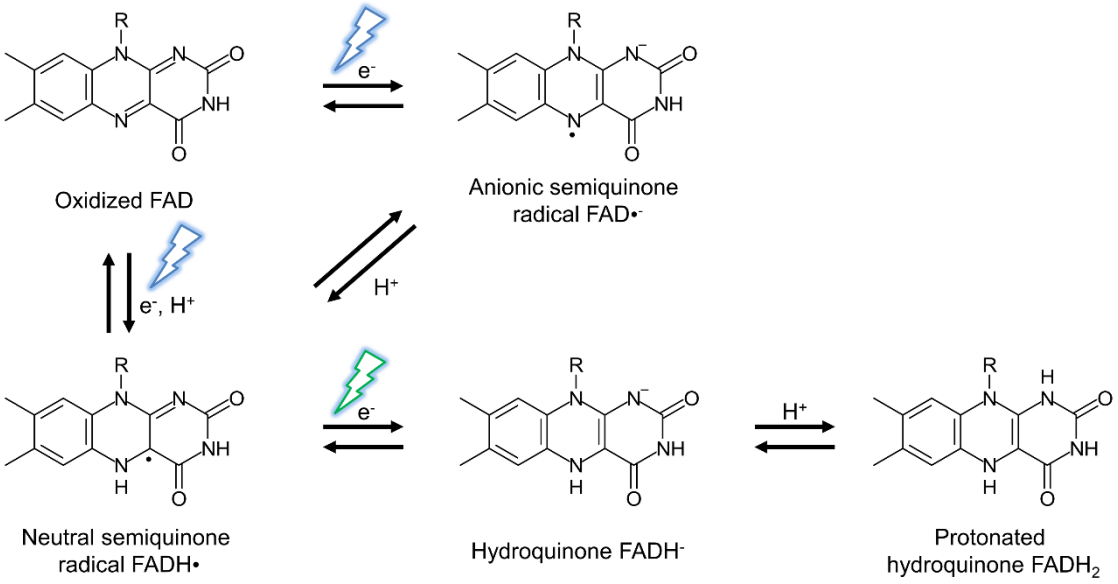

Figure 1-5. Light-induced chemical reactions of the chromophore FAD.

1.4 Purpose of the present study

Axon guidance is a crucial step for the nervous development. Although the biomolecular signaling mechanisms have been intensively investigated in cultured neurons, it is hard to examine the modulation in living tissue due the lack of tools. The potential of the regulation of axon guidance with light is expected to facilitate the direct analysis of the interplay between the growth cones and the extracellular environments. On the other hands, there is a huge latent need for controlling the orientation of the extending axons from implanted neurons in regenerative therapies for nervous disorders. Collectively, it is required to develop a novel optogenetic system that modulates the activity of guidance receptors for controlling neurite outgrowth direction.

Here, I aimed to develop an optical system to control the direction of neurite outgrowth by photo-activating DCC, an axon guidance receptor. Because the ligand-induced oligomerization of DCC is crucial for the activation of intracellular signaling to induce cytoskeletal remodeling[81], DCC was genetically with CRY2, which forms oligomer upon light absorption.

At first, photo-activation of DCC with CRY2 was confirmed in non-neuronal cells. Then, the ability of the developed system to navigate axon with light was examined in cultured neurons. Finally, the applicability for the *in vivo* light-induction of growth cone turning was demonstrated in the nematode *Caenorhabditis elegans*.

Chapter 2.

Materials and Methods

2.1 Strains and culture

The *C. elegans* nematode was maintained using standard techniques[82]. The following lines were used in this thesis; MT464 *unc-5(e53)* IV; *dpy-11(e224)* V; *lon-2(e678)* X, MT5013 *ced-10(n1993)* IV, NW434 *unc-6(ev400)* X, EG1285 *lin-15(n765); oxIs12[Punc-47::gfp; lin-15(+)]* X, JN1900 *unc-5(e53)* IV; *unc-6(ev400)* X; *peEx1900[Punc-47::PA-UNC-40::venus; Punc-47::mCherry; Plin-44::gfp]*, and JN1901 *unc-5(e53)* IV; *unc-6(ev400)* X; *peEx1901[Punc-47::mCherry; Plin-44::gfp]*, JN1902 *ced-10(n1993) unc-5(e53)* IV; *unc-6(ev400)* X; *peEx1900[Punc-47::PA-UNC40::Venus; Punc-47::mCherry; Plin-44::gfp]*. MT464, MT5013, NW434 and EG1285 were obtained from Caenorhabditis Genetics Center (MN, USA). Extrachromosomal arrays were generated by microinjections[83] with co-injection marker *Plin-44::gfp*. The double mutant was confirmed by phenotypes and PCR genotyping.

2.2 Plasmid construction

The cDNAs of DCC and FAK were amplified by PCR from *Mus musculus* brain cDNA mixture (GenoStaff Co. Ltd., Tokyo, Japan), and that of CRY2 was from pGal4BD-CRY2 (Addgene, MA, USA). The UNC-40 cDNA was generated by RT-PCR from total *C. elegans* RNA mixture. Amino acid GS linker, V5 , myc and FLAG were generated by oligonucleotides overlapping with each other. Additional mutation for CRY2 (D387A) was introduced by PCR. The PCR products (DCC, CRY2, CRY2 (D387A)) were inserted into pcDNA4 V5/His ver. B vector (Invitrogen Corp., CA, USA) or pcDNA3.1 myc/His ver. B vector (Invitrogen Corp.). FLAG tagged FAK was subcloned into pcDNA4 vector. For optimal expression in chick DRG neurons, cDNAs of V5 tagged PA-DCC and mCherry were cloned under the CAG promoter in

the pCAGGS vector (provided by J. Miyazaki, Osaka University, Osaka, Japan). In experiments for *C. elegans*, cDNAs encoding PA-UNC-40::Venus and mCherry were subcloned under the *unc-47* promoter by the GATEWAY system (Invitrogen Corp.)[84].

2.3 Cell culture and transfection

For expression in Human embryonic kidney (HEK293) T cells, the cDNAs were transfected by Lipofectamine 2000 (Invitrogen Corp.) according to the manufacturer's protocol. The transfected cells were maintained in Dulbecco's Modified Eagle Medium (DMEM, high glucose; Wako Pure Chemical Inds. Ltd., Japan) with 10% Fetal Bovine Serum (FBS; Gibco, CA, USA) at 37 °C in 5% CO_2. For expression in chick DRG neurons dissected from E9 embryos, the expression vectors were introduced by electroporation (neon; Invitrogen Corp.). The neurons were suspended in RPMI1640 medium (Gibco) with 10% FBS and 40 ng mL^{-1} NGF (Promega Corp., WI, USA), at the concentration of 400,000 neurons mL^{-1}. 50 μL droplets were placed on the lids of 100 mm dishes and incubated for 3 days at 37 °C in 5% CO_2 to generate neuron balls. The neuron balls were transferred individually to glass base dishes coated with poly-D-lysine and mouse laminin (Invitrogen Corp.). The placed neuron balls were cultured for 24 h in RPMI1640 medium with 10% FBS and 20 ng mL^{-1} NGF.

2.4 Immunocytochemistry

For HEK293T cells, the medium was exchanged with 4% paraformaldehyde at 37 °C for 20 min. The cells were permeabilized with 0.2% Triton X-100 in PBS at room temperature for 20 min. After washing with PBS, the cells were blocked with 0.2% gelatin from cold water fish skin

(FSG; Sigma-Aldrich Corp., MO, USA) in PBS for 1 h at room temperature or overnight at 4 °C. The blocked cells were incubated with mouse anti-V5 antibody (1:4000, novex, CA, USA) in PBS (0.2% FSG) for 2 h at room temperature, shaking gently. After washing with PBS, the cells were immunostained with Alexa-Fluor 488 conjugated donkey anti-mouse IgG antibodies (1:2000, GE Healthcare, WI, USA) in PBS (0.2% FSG) for 1 h at room temperature. The cells were washed with PBS and mounted with FluorSave (Calbiochem) on a slide glass. Images were taken on a confocal fluorescent microscope (FV-1000D; Olympus Corp., Tokyo, Japan).

For DRG neurons, 4% paraformaldehyde 4% Sucrose was used for fixation at room temperature for 20 min. The neurons were permeabilized with 0.1% Triton X-100 in PBS for 10 min and blocked with 5% goat serum (Vector Laboratories, CA, USA) 0.01% Triton X-100 in PBS for 1 h. The blocked neurons were incubated with mouse anti-V5 antibody (1:1000, novex) or anti-FAK [pY397] antibody (1:500, GeneTex, CA, USA) in Can Get Signal Immunoreaction enhancer solution (TOYOBO, Osaka, Japan). After washing with PBS (0.01% Triton X-100), the neurons were immunostained with Alexa-Fluor 488 conjugated donkey anti-mouse IgG antibodies or Alexa-Fluor 647 conjugated goat anti-rabbit IgG antibodies (1:2000, GE Healthcare) in PBS (1% goat serum, 0.01% Triton X-100) for 1 h at room temperature. The neurons were washed with PBS (0.01% Triton X-100) and mounted with ProLong Diamond (Invitrogen Corp.). Images were taken on a confocal fluorescent microscope (FV-1000D).

2.5 Western blot analysis

Transfected cells were illuminated with LED light (0.05–5 mW cm^{-2} at 440 nm, Optocode Corp., Tokyo, Japan) for 1–15 min. The other cells were incubated with or without recombinant mouse netrin-1 (200 ng mL^{-1}; R&D Systems, MN, USA) for 15 min in the dark. The stimulated

cells were collected with PBS. After removal of the supernatant by centrifugation at 4°C, the cells were lysed in the PLC buffer (10% glycerol, 1% Triton X-100, 150 mM NaCl, 100 mM NaF, 50 mM HEPES, 10 mM NaPPi, 1.5 mM $MgCl_2$, 1 mM EGTA, 1 mM Na_3VO_4 and protease inhibitor Complete (Roche, Switzerland), pH 7.5). The lysates were boiled with the sample buffer (25% glycerol, 10% SDS, 5% 2-mercaptoethanol, 0.02% Bromophenol Blue, 250 mM Tris–HCl, pH 7.6) at 95 °C for 5 min.

The co-IP assay was performed by referring to the previous report that detected the transient CRY2-CIB1 interaction with light[85]. Before the assay, 1 μL of mouse anti-V5 antibody was mixed with 50 μL of Protein G sepharose (GE Healthcare) in PLC buffer at 4 °C for 2 h. Cells with or without illumination were lysed in PLC buffer. After centrifugation, the supernatant was incubated with the pre-mixed anti-V5 antibody at 4 °C for 30 min with rotation. The mixture was washed quickly using ice-cold PLC buffer for four times and collected by centrifugation. 5× sample buffer was added to the sample and boiled at 95 °C for 5 min. Protein G sepharose were removed by centrifugation.

The samples were separated by SDS-PAGE and transferred to nitrocellulose membrane (GE Healthcare). The membrane was blocked with 1% skimmed milk or 2% ECL Advance Blocking Agent (GE Healthcare) in Tris-buffered saline containing Tween-20 (TBS-T; 0.05% Tween-20, 150 mM NaCl, 50 mM Tris-HCl, pH 8.0) for 1 h. The membrane was washed briefly using TBS-T and reacted with each specific antibody; mouse anti-βActin (1:5000), mouse anti-FLAG (1:4000, Sigma-Aldrich Corp.), rabbit anti-PLCγ-1 [pY783] (1:2000), mouse anti-myc (1:4000, Cell Signaling Technology, NA, USA), mouse anti-PLCγ-1 (1:2000, Upstate Biotechnology, NY, USA), rabbit anti-FAK [pY397] (1:2000) (Invitrogen Corp.). Anti-rabbit IgG and anti-mouse IgG labeled with horseradish peroxidase (1:5000, GE Healthcare) were used as secondary antibodies. The immunoblot bands were detected using SuperSignal West Femto Substrate (Thermo

Scientific, IL, USA) with an image analyzer (LAS-1000 plus; Fuji Photo Film Co. Ltd., Tokyo, Japan).

2.6 Observation of light-induced aggregation

Transiently transfected COS-7 cells were observed by an inverted epifluorescence microscope (IX81; Olympus Corp.) with objective lens (UPlanApo 100×; Olympus Corp). Whole cell area was illuminated with a blue light (metal halide lamp with 425–440 nm filter, 8 nW sample-site beam power at 440 nm, 10 s min^{-1} pulses for 15 min). mCherry fluorescence images were acquired with a EM-CCD camera (iXon DV887; Andor Technology Ltd., Northern Ireland, UK).

2.7 Growth cone turning assays in chick DRG neurons

The medium for culturing neuron balls was exchanged with Leibovitz's L-15 medium (Gibco) with N-2 (Gibco), 750 μg mL^{-1} bovine serum albumin (Gibco), 20 ng mL^{-1} NGF, and 40 μM Sp-cAMPS (Calbiochem) and incubated for 30 min at 37 °C in 5% CO_2. The neurons were observed under an inverted microscope (IX81; Olympus Corp.) with objective lens (UPlanApo 100×; Olympus Corp). An area within one side of the growth cone was illuminated with light (metal halide lamp with 425–440 nm filter, 8 nW sample-site beam power at 440 nm, for 5 s every 5 min pulses). The illuminated area was approximately 5μm diameter in diameter, which was modulated by a pinhole. During assays, differential interference contrast (DIC) images of the growth cone were obtained with a CCD camera (CoolSNAP ES; Roper Scientific Inc., NJ, USA). The illumination methods were based on the previous reports[86, 87]. Growth cone turning was

evaluated by calculating the turning angles. The procedure is as follows (**Figure 2-1**): trace the growth cone center defined as the intersection of the distal edge of the growth cone central domain and the extrapolated line from the axon. Define the original direction of axon extension by a straight line connecting the positions of the growth cone at the onset and 5 min before photo-activation. Define the direction after the stimulation as a straight line connecting the positions of the growth cone at the onset and at the end of repetitive stimulation. The growth cone turning angles were then calculated by the angle between the original direction and the direction after the stimulation. Only growth cones with net extension over 6 μm were included for analysis.

2.8 Analysis of axon guidance defects in *C. elegans*

VD/DD neurons in *C. elegans* were visualized with an *Punc-47::mCherry* or *Punc-47::GFP* transgene, which were previously reported to be expressed in all GABAergic neurons[88]. VD/DD axons were defined as guidance defective when they branched, or turned at an angle greater than 45°, or failed to reach the dorsal nerve cord.

2.9 Analysis of growth cone attraction in *C. elegans*

Eggs were collected by lyse adult worms with an alkaline-bleach solution. The collected eggs were incubated in the M9 buffer at 20 °C. Hatched L1 worms were transferred to NGM plates with OP50 seeding and grown at 20 °C until the worm became L2. The worms were placed into M9 droplet with 0.02% levamisole (Sigma-Aldrich Corp.) on the glass base dish. A 5% agarose pad was placed on the droplet and wet paper was set inside the dish to maintain humidity. The worms were observed under a confocal microscope within 3 h. To exclude stalled growth cones, lamellipodia ruffling in growth cones were confirmed 10 min before the illumination. The

growth cone was illuminated with 0.1% 20 mW LD 488 nm laser light at 2.0 μs pixel^{-1}. Centroids of growth cones and the intensities of fluorescence were calculated using ImageJ software.

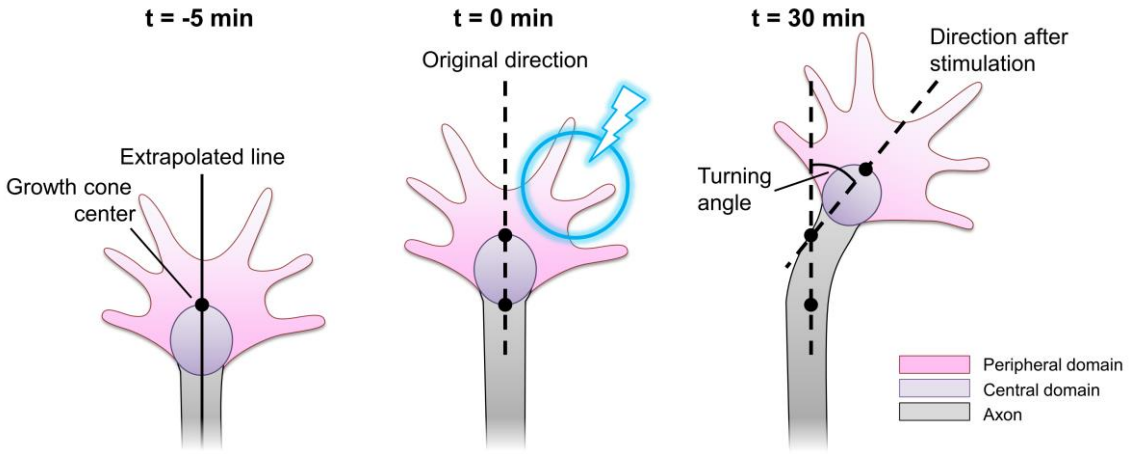

Figure 2-1. Definition of the turning angle.

Black dots indicate the growth cone centers. The solid line represents the extrapolated line from the axon. Dotted lines show the directions of axonal elongation before and after the illumination.

Chapter 3.

Development of an optical system to control the axonal outgrowth direction

3.1 Light-dependent activation of PA-DCC molecules

For the development of an optical system, it is important to reduce the basal oligomerization level of the engineered DCC protein in a dark state. In a previous report, the attachment of GFP to the N-terminus of CRY2 disturbs weak or transient self-association with endogenous CRY2 without disturbing light-induced cluster formation[89, 90]. Accordingly, the C-terminal cytoplasmic tail of DCC was connected with the N-terminus of CRY2 via a flexible GS linker (GGRGGGGSGGGGS), resulting in a protein named PA-DCC (**Figure 3-1a**). Because of the light-dependent CRY2 oligomerization, fused DCCs undergo oligomerization and consequent activation, leading to axonal attraction (**Figure 3-1b**).

To investigate the oligomerization of PA-DCC upon light stimulation, myc or V5 epitope tag was attached to the PA-DCC for co-immunoprecipitation (co-IP). DCC connected with photo-insensitive CRY2 mutant (D387A)[85], represented as PA-DCC (D387A), and DCC without CRY2 named "DCC" were also prepared as a non-light reactive control (**Figure 3-1a**). V5 and myc tagged molecules were co-expressed in HEK293T cells, which do not express endogenous DCC[91]. Plasma membrane localization of the expressed molecules was confirmed using confocal microscopy (**Figure 3-2**). Cells co-expressing the tagged molecules were exposed to blue light (5 s min^{-1}) for 15 min before co-IP assay. The protein samples were immunoprecipitated by anti-V5 antibody. If the protein forms oligomer, myc-tagged molecules are also pulled down. The precipitated samples were analyzed with anti-myc antibody to examine the co-immunoprecipitation of the myc-tagged molecules (**Figure 3-3a**). Myc-tagged molecules were detected in the sample of V5-tagged PA-DCC molecules upon the blue light illumination. In the case of V5-tagged DCC and PA-DCC (D387A), the myc-tagged molecules were not detected. The light-induced oligomerization efficiency of PA-DCC increased along with the illumination

time (**Figure 3-3b** and **c**), light intensity (**Figure 3-3d** and **e**), and the pulse number **(Figure 3-3f** and **g**). Collectively, these results indicate that photo-conversion of CRY2 triggered PA-DCC oligomerization. To examine whether PA-DCC forms visible light-induced aggregation, which was observed in CRY2 PHR domains[92], illuminated cells expressing PA-DCC molecules were observed under epi-fluorescence microscope. However, the light-induced PA-DCC aggregation was not detected using epifluorescence microscopy, whereas CRY2 PHR-mCherry-caax formed visible aggregation upon light illumination (**Figure 3-4**). These observation suggest that the size of the PA-DCC oligomer is smaller than the optical resolution. Taken altogether, PA-DCC molecules forms oligomer, which is not large enough to visualize under epifluorescence microscope.

Netrin-1, a diffusible attractive guidance protein, binds to an extracellular domain of DCC, resulting in DCC oligomerization[11, 93]. A cytoplasmic P3 domain of DCC mediates its oligomerization and also interacts with signaling proteins such as Focal Adhesion Kinase (FAK)[94] and phosphatidylinositol transfer protein α[95]. Upon netrin-1 binding, these interactions respectively trigger the phosphorylation of FAK and PLCγ-1, initiating the downstream signaling cascade for axon turning. To investigate whether light-dependent oligomerization of PA-DCC trigger the signaling, phosphorylation levels of FAK and PLCγ-1 were examined. Results confirmed that FAK and PLCγ-1 in PA-DCC expressing cells were phosphorylated with blue light illumination, although light illumination on the cells without PA-DCC expression did not induce their phosphorylation (**Figure 3-5a**). Additionally, the phosphorylation levels of FAK elevated with increasing number of light pulses (**Figure 3-5b** and **c**), indicating that the extent of the activation is tunable by the light dose. These results demonstrate that light-induced CRY2 oligomerization can trigger the DCC activation.

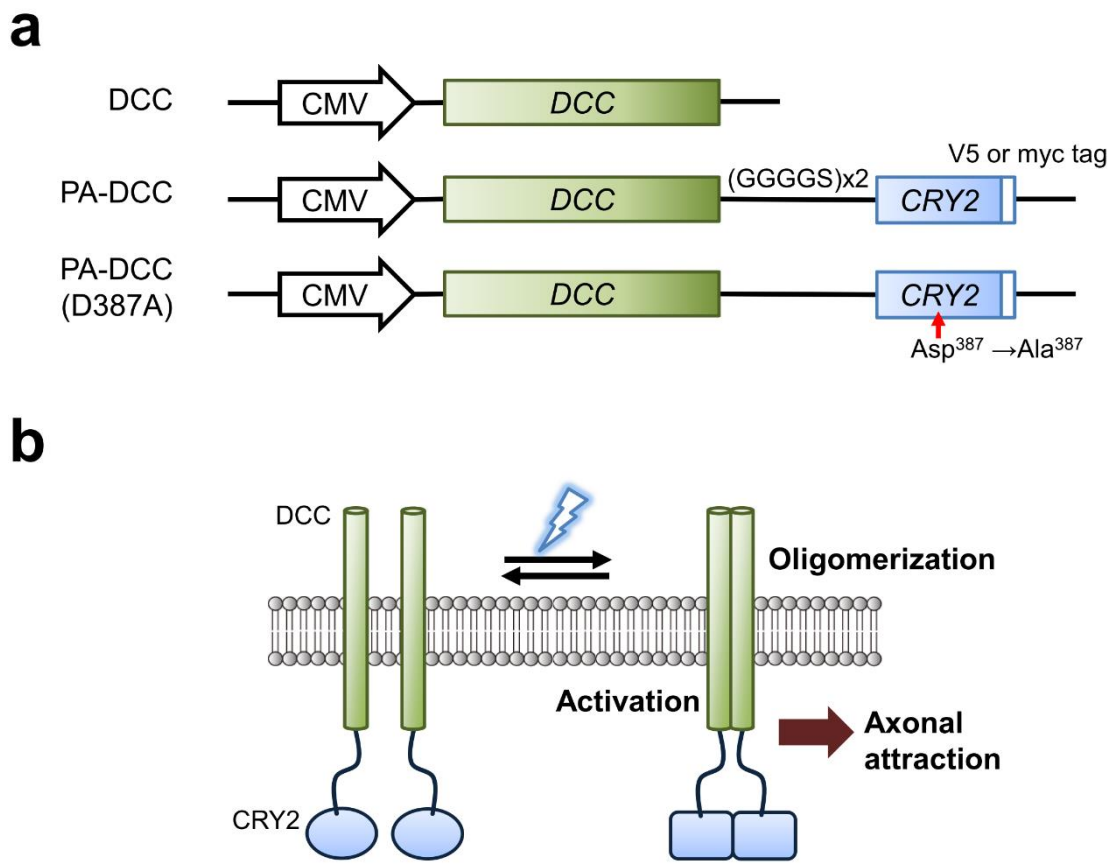

Figure 3-1. Schematics for the structures and photo-activation model of PA-DCC.

(**a**) Domain structures of PA-DCC molecules. All text in italics refers to the genes of their corresponding proteins. CMV represents a promoter for gene expression. DCC is connected with CRY2 via GS linker (GGRGGGGSGGGGS). White squares show epitope V5 or myc tags. (**b**) Schematic diagram for the strategy of DCC activation with blue light illumination.

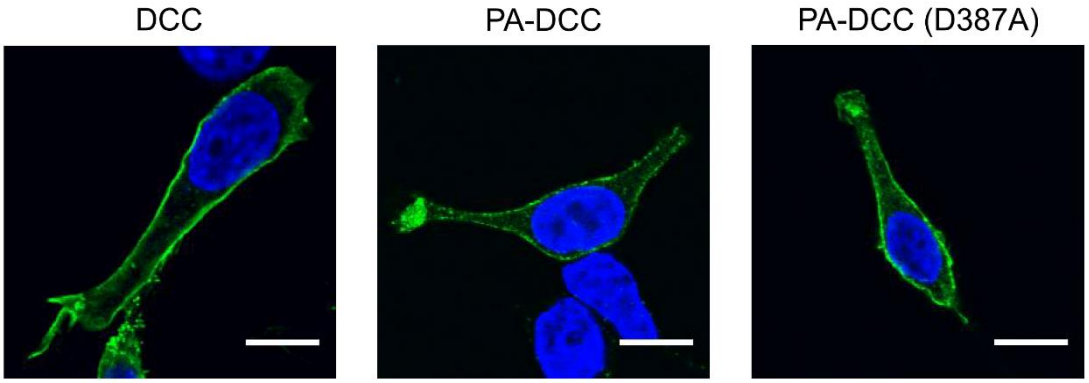

Figure 3-2. Localization of DCC-containing molecules in HEK293T cells.
Each molecule was immunolabeled with Alexa488 (green) using V5-epitope tag in fixed cells. Nucleus was stained with Hoechst33342 (blue). Scale bar, 10 μm.

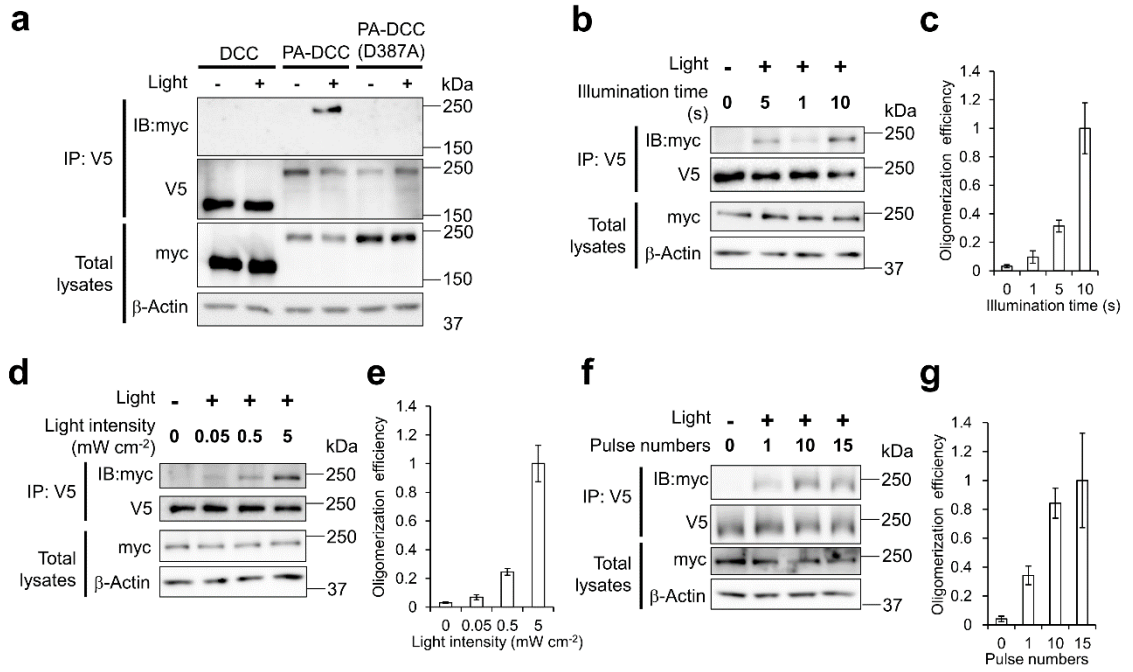

Figure 3-3. Light-induced oligomerization of PA-DCC.

(**a**) Confirmation of DCC oligomerization. Cells co-expressing myc-tagged and V5-tagged molecules were lysed after illumination (10 s min^{-1} pulses for 15 min). V5-tagged molecules were immunoprecipitated from the lysates with the anti-V5 antibody (IP: V5). Co-immunoprecipitated myc-tagged molecules were detected by anti-myc antibody (IB: myc). (**b, c**) Dependence of PA-DCC oligomerization efficiency on the illumination time. Cells were lysed after illumination (1, 5 or 10 s min^{-1} pulses for 15 min). A representative data was shown in **b**. The efficiency was calculated for each illumination time and indicated as scores relative to the maximal value in **c**. Error bars, SEM (n = 3). (**d**, **e**) Light intensity dependency of the oligomerization. Cells were lysed after illumination (10 s min^{-1} pulses for 15 min). Error bars, SEM (n = 3). (**f**, **g**) Pulse number dependency of PA-DCC oligomerization. Cells were lysed after illumination (10 s min^{-1} pulses for 1, 10 or 15 min). Error bars, SEM (n = 3).

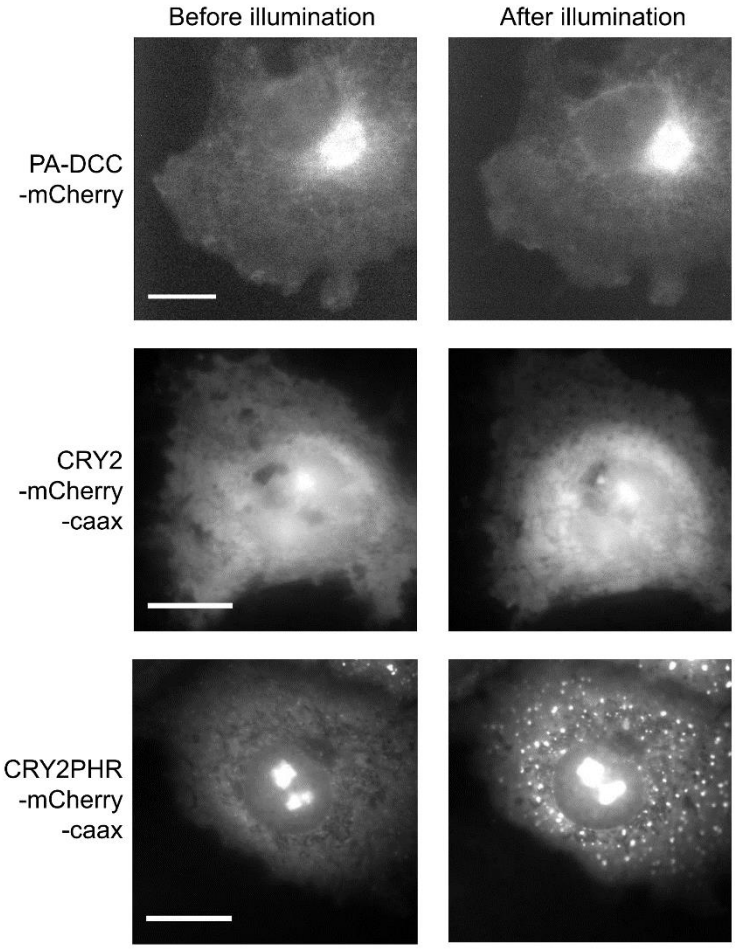

Figure 3-4. Detection of light-induced aggregation of CRY2 fused molecules.
Epifluorescence images of COS-7 cells expressing CRY2 or CRY2 PHR domain fused molecules were acquired before and after illumination (10 s min^{-1} pulses for 15 min). Scale bar, 20 μm.

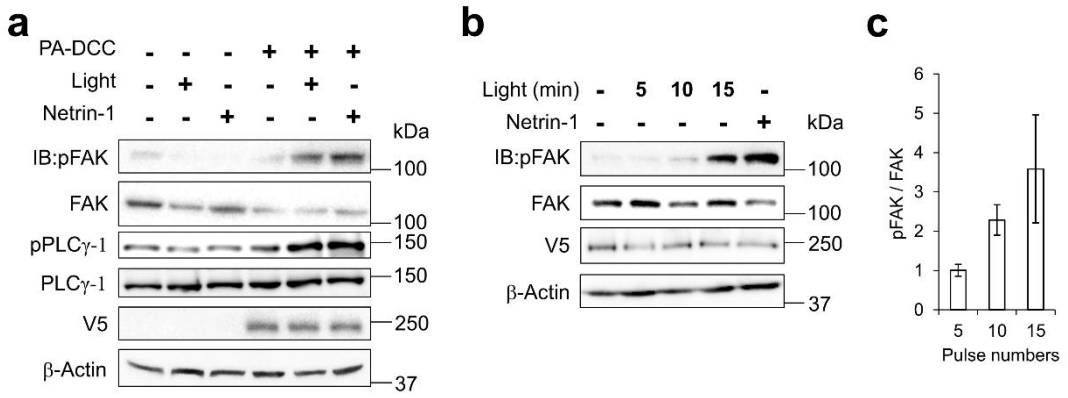

Figure 3-5. Activation of PA-DCC with blue light.

(**a**) Analysis of the phosphorylation of FAK and PLCγ-1. Cells were stimulated with light or with netrin-1 (200 ng mL^{-1}) for 15 min. Each protein or phosphorylation was detected by the specific antibody. (**b**, **c**) Pulse number dependency of the FAK phosphorylation. A representative data was shown in **b**. Phosphorylation level was indicated as scores relative to the basal level in **c**. Error bars, SEM (n = 4).

3.2 Reversibility of PA-DCC activation

To confirm the reversibility of light-dependent activation of PA-DCC, the dissociation profile after light illumination of PA-DCC was investigated. Light-exposed cells expressing PA-DCC were incubated in the dark before assays. The results of co-IP showed that oligomerized PA-DCCs disappeared along with the elapsed time after illumination (**Figure 3-6a** and **b**). Most PA-DCCs dissociated within 10 min. The reversion to dark state has a half-life of 76 ± 8 s, which corresponded to the previous report using purified CRY2[96]. Accordingly, the phosphorylated FAK in the cells decreased gradually over time (**Figure 3-6c** and **d**). The time course of PA-DCC deactivation corresponded to that of the dissociation of the PA-DCC molecules after the illumination. These results indicate that blue light illumination activates PA-DCC transiently, thereby ensuring the capability of the tool to guide axons to the desired direction with repetitive illumination on growth cones.

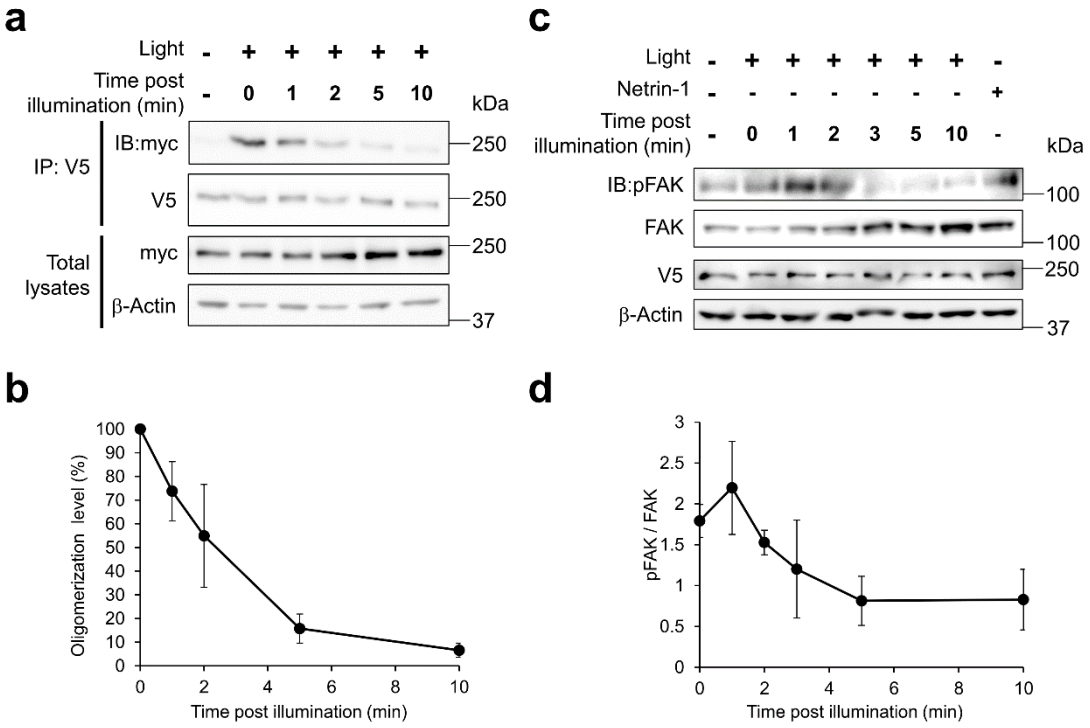

Figure 3-6. Reversibility of PA-DCC activation.

(**a, b**) Dissociation profiles of PA-DCC oligomer. Light-illuminated cells were incubated for each indicated time. The proteins were isolated by IP with anti-V5 antibody. Co-immunoprecipitated myc-tagged PA-DCC was visualized using Western blotting. A representative data was shown in **a**. The oligomerization level was indicated relative to the level just after the illumination in **b**. Error bars, s.d. (n = 3). (**c, d**) Dephosphorylation of FAK after light illumination. Cells were illuminated and incubated in a dark condition for the indicated time. The cell components were analyzed with each antibody. A representative data was shown in **c**. The phosphorylation level was indicated relative to the basal level in **d**. Error bars, s.d. (n = 3).

3.3 Axonal attraction by light-induced PA-DCC activation

To explore the possibility of the axonal attraction with PA-DCC, growth cone turning assays were performed in DRG neurons from chick embryos (E9). cDNA encoding PA-DCC under control of the expression CAG promoter (**Figure 3-7a**) was transfected to DRG neurons. It was confirmed that PA-DCC localized on the cellular membrane at the area of growth cone (**Figure 3-7b**). The transfected DRG neurons were plated on dishes coated with extracellular matrix protein, lamin-1. To suppress the influence of laminin-1-dependent decreases in the cytoplasmic cAMP/cGMP level in the growth cones, the neurons were treated with Sp-cAMPS, an activator of cAMP-dependent kinase, before each assay[20, 23]. A part of transfected growth cones was illuminated with blue light in a pulse-like manner (5 s every 5 min) during the observation. Light-induced axonal attraction was clearly observed in neurons expressing PA-DCC (**Figure 3-8a**). In contrast, the blue light illumination did not affect the axonal growth direction without PA-DCC expression or with light-insensitive PA-DCC (D387A). Time lapse imaging of the light-induced axonal attraction revealed the clear growth cone movements in response to the pulsatile illuminations (**Figure 3-8b**). From the results, a cumulative distribution of final growth cone turning angles was analyzed (**Figure 3-9a**). In most of the assays (14 out of 16), growth cones expressing PA-DCC turned at an angle of greater than 25°. The mean turning angle of growth cones with PA-DCC expression was 37.4 ± 3.8°, which was significantly different from that of growth cones without PA-DCC expression (-0.6 ± 3.3°) (**Figure 3-9b**).

After the light-induced attraction, the illumination area was repositioned from the left side to the right side. Also, the pulse-like illuminations continued further (**Figure 3-10a**). Statistical analysis revealed that all examined growth cones, which were attracted by the first illumination at the angles of -26.2 ± 4.4°, turned to the repositioned illuminated side at the angles of 39.2 ±

7.0° upon subsequent illumination. The results demonstrate the capability of redirecting the growth cone with repeated light-induced turning.

To confirm that the illumination on a part of the growth cone triggered attractive signaling locally, phosphorylation of FAK within illuminated growth cones were examined by immunocytochemistry (**Figure 3-11a**). Compared to the growth cone without PA-DCC, FAK phosphorylation signals increased in the illuminated side, including in filopodia (**Figure 3-11b**). In the absence of Sp-cAMPS treatment, light-induced axon repulsion was observed (**Figure 3-8a**, **Figure 3-9a** and **b**). Considering that the reduction of the cAMP/cGMP level converts axonal attraction to axon repulsion in netrin-1/DCC signaling[23], the obtained results collectively suggest that CRY2-mediated oligomerization of PA-DCC upon light illumination triggered the downstream signaling pathway of DCC. Therefore, PA-DCC can control the neurite outgrowth direction with light illumination in chick DRG neurons.

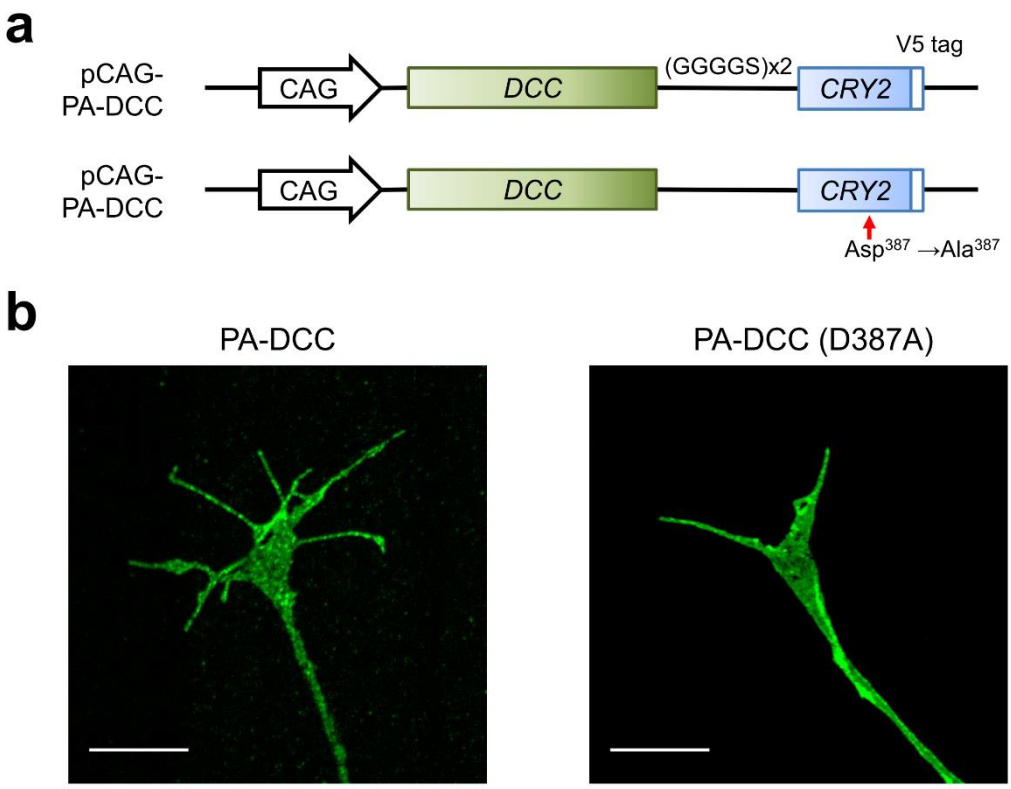

Figure 3-7. PA-DCC molecules for experiments in chick DRG neurons.

(**a**) Domain structures of PA-DCC molecules. All text in italics refers to the genes of their corresponding proteins. CAG represents a promoter for gene expression. DCC is connected with CRY2 via GS linker (GGRGGGGSGGGGS). White squares show epitope V5. (**b**) Localization of PA-DCC and PA-DCC (D387A) in chick DRG neuron. Each molecule was immunolabeled with Alexa488 (green) using V5-epitope tag in fixed neurons. Scale bar, 10 μm.

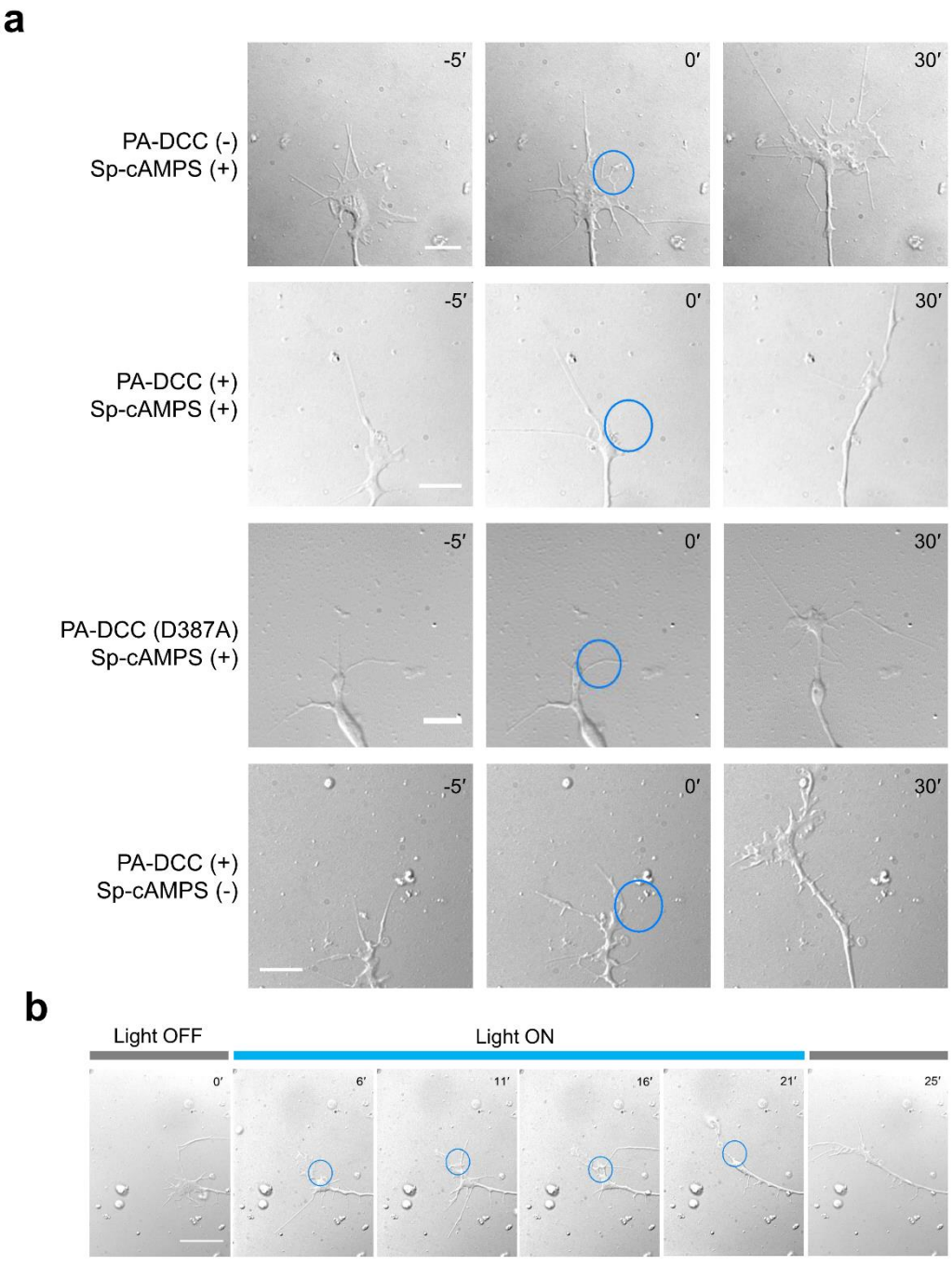

Figure 3-8. Light-induced growth cone turning of chick DRG neurons expressing PA-DCC. (**a**) DIC images of illuminated growth cones. Blue circles represent illuminated regions (5 s every 5 min pulses for 30 min). Digits show the minutes after the onset of the illumination. Scale bar, 5 μm. (**b**) Time lapse images of light-induced growth cone attraction with PA-DCC. Digits show elapsed minutes. The illuminations were performed at t = 6, 11, 16, 21 min. Scale bar, 10 μm.

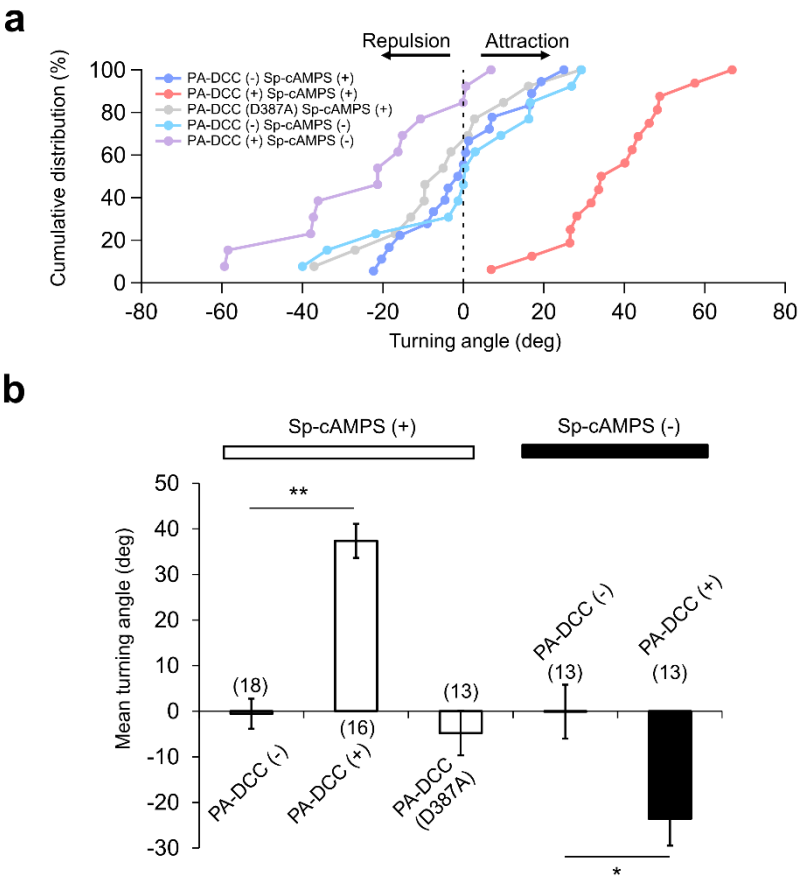

Figure 3-9. Turning angle analysis of illuminated growth cones.

(**a**) Cumulative distribution of final growth cone turning angles in the light-induced growth cone attraction assay with or without Sp-cAMPS treatment. Turning angles were calculated based on the original definition explained in Chapter 2. (**b**) Averaged turning angles of growth cones with illumination. Numbers in parentheses indicated the total number of growth cones tested. Error bars, SEM. Statistical significance was determined by one-way ANOVA followed by Dunnett's test for multiple comparison, $^{**}P < 0.01$; or by *t*-test, $^{*}P < 0.05$.

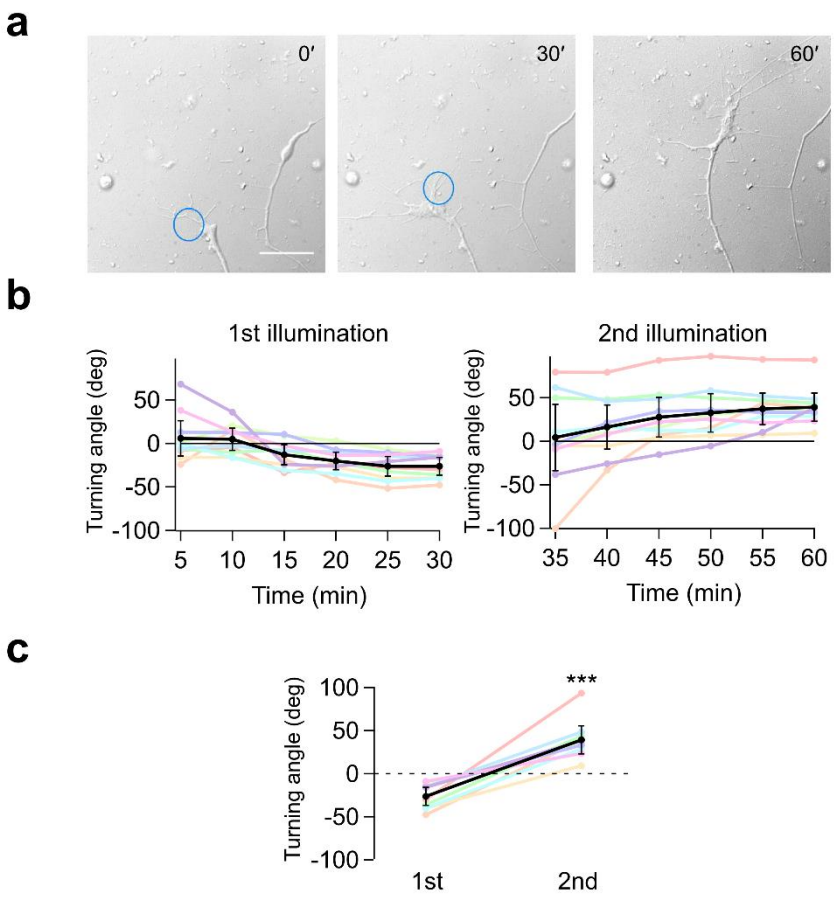

Figure 3-10. Repositioned illuminations caused repeated light-induced growth cone attraction to different directions.

(**a**) A representative data of the repeatedly illuminated growth cones. Scale bar, 10 μm. (**b**) Time course turning angle analysis of growth cones with repositioned illuminations. Each data is shown by a colored line. Averaged data are shown as black. The turning angles with positive values represents growth cones turning to the right side. Error bars, 98% confidential intervals of the mean (n = 10). (**c**) Final turning angles of each growth cone before and after repositioned illuminations in **b**. Each experimental trial is shown with the same colored line as in **b**. Averaged data are shown as black. Error bars, 98% confidential intervals of the mean (n = 10). ***P < 0.005, paired t-test.

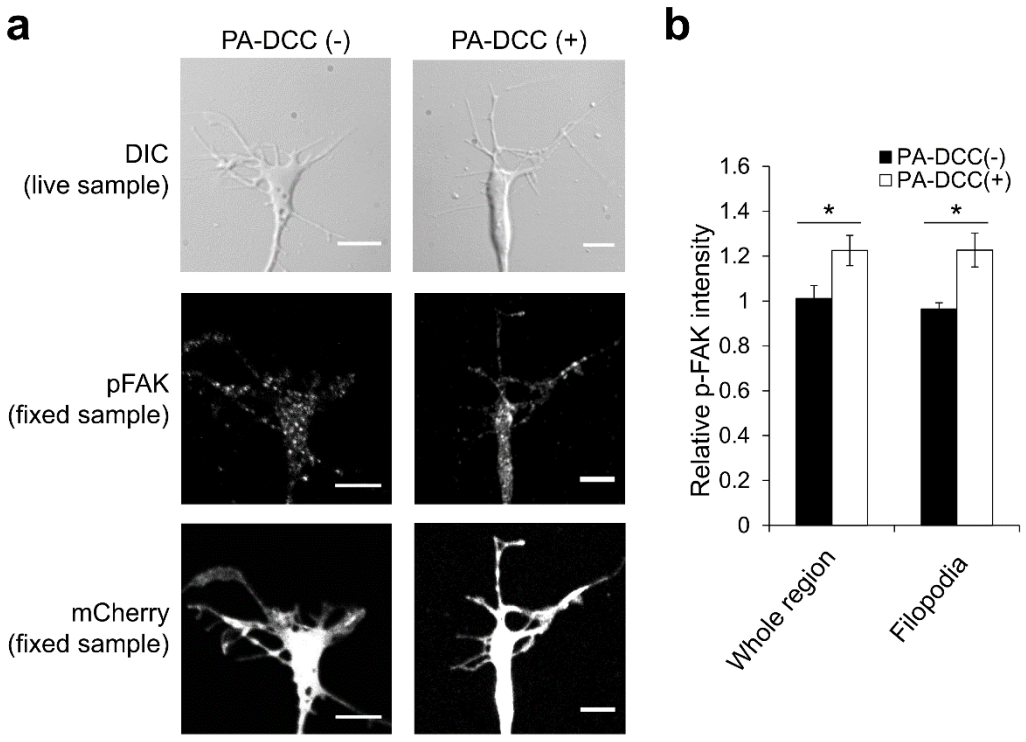

Figure 3-11. Local phosphorylation of FAK.

(**a**) Transmitted, fluorescence and immunostained images of growth cones. A part of chick DRG growth cones with or without PA-DCC was illuminated with blue light (5 s every 5 min pulses for 15 min). Growth cones were fixed just after the third illumination and immunostained with the specific antibody. The right sides of the growth cones were illuminated. Scale bar, 5 μm. (**b**) Analysis of FAK phosphorylation level in the illuminated side. Mean phosphorylation intensity in the illuminated side was indicated as scores relative to the intensity in the non-illuminated side. pFAK intensity was normalized by mCherry fluorescence. Error bars, SEM (n = 5). *P < 0.05, unpaired t-test.

3.4 Discussion

Light-induced oligomerization system can activate the axon guidance receptor DCC in a form of CRY2 fused molecule, PA-DCC, as demonstrated herein. PA-DCC transiently formed oligomer upon light illumination on the membrane, which triggered downstream signaling for axonal attraction in the illuminated side of the growth cones.

All previous light-induced oligomerization system based CRY2 used only the PHR domain[66, 68, 70, 92]. In contrast to the PHR domain, epifluorescence observations showed that PA-DCC using full length of CRY2 formed no large visible oligomers in my experimental setup. Considering that full length CRY2-mCherry-caax also failed to form visible aggregation upon light stimulation, I infer that it is attributable to the character of the full length CRY2. Regarding the dissociation kinetics, a half-life of the full length CRY2 (~1.3 min) was shorter than that of the PHR domain (~5.5 min)[66]. The developed full length CRY2 based light-induced oligomerization system would be useful if the experiments prefers lower aggregation efficiency or the faster dissociation, although the further investigation for the precise comparison of the two systems is still required.

Endogenous DCCs normally form oligomer upon binding with the attractive guidance molecule, netrin-1. Recent X-ray crystal structural analysis showed that netrin-1 serves as a scaffold for local DCC assembly via its two receptor-binding sites[11]. However, it remains unclear whether netrin-1 binding induces a conformational change in DCC for the activation. In this study, we demonstrated for the first time that DCC oligomerization is sufficient for evoking the growth cone turning. The results suggest that the oligomerization is a key step in the DCC activation, which is consistent with the fact that overexpression of DCC typically engenders their activation without netrin-1[94]. Light-induced local activation of DCC eventually attracted growth cones

without mechanically tethered guidance cue molecules. Indeed, the physical attachment of netrin-1 to the substrate, extracellular matrix or dishes, plays a key role in the induction of the attractive response[17]. However, considering that PA-DCC molecules are not physically tethered to any substrate during the light-induced attraction, the experimental finding suggests that the substrate attachment of netrin-1 is not necessary for the growth cone attraction. Nevertheless, it might be important at a physiological level of netrin-1 concentration.

Intracellular signaling in axon guidance is modulated by extracellular matrix. As demonstrated, the light induced attraction with PA-DCC was repulsive signaling by the laminin-1-induced reduction of cAMP/cGMP ratio. Therefore, the photo-activating system of the axon guidance receptors can analyze the extracellular matrix-mediated modulation of intracellular signaling, which is especially important in living organisms where the surrounding environments are composed of heterogeneous extracellular matrix proteins.

Optical modulation of biological phenomena in living cells is sometimes accompanied by adverse effects of the light itself. In cultured neurons, it was recently reported that light-induced warming with near-IR laser can repel growth cones[97]. For effective local heating with laser light, high light dose (100 mW μm^{-2} for more than 10 min) and long wavelength (>700 nm) are necessary. In contrast, such photo-thermal effects are negligible in the developed method because the developed photo-reactive molecules are activated with low dosage of light (0.07 nW μm^{-2} for 5s every 5 min) and shorter (425–440 nm) wavelength. Moreover, light illumination itself did not affect the original neurite outgrowth direction in the same condition. Collectively, the light-induced attraction with PA-DCC is dependent on the activation of DCC signaling, not on the light illumination itself.

DCC is only one of the various guidance receptors involved in the neural circuit formation. During nervous system development, numbers of ligand/receptor signaling pathways dynamically

cooperate mutually to achieve highly complicated neural wirings without errors[98]. Considering that the light illumination activates the receptor of interest in the developed system specifically, it is also possible to expand the system for photo-controlling the function of other guidance receptors with similar activation mechanisms, such as UNC-5, which mediates short-range repulsion in a homodimer[99].

One of the great advantage of the optical stimulation system is that it is readily applicable to the *in vivo* experiments. Developing axons in living organisms are surrounded by heterogeneous extracellular environments which affects the motility of growth cones. The potential of the axonal photo-attraction system developed in this chapter for the *in vivo* analysis of growth cone motility will be investigated in the **Chapter 4** of this thesis.

3.5 Conclusion

In conclusion, I developed an optical system that enables direct modulation of the neurite outgrowth direction by activating axon guidance receptor DCC with light-oligomerizing system. The photo-attraction system successfully demonstrated the repeatability of the light-induced axonal attraction. It ensures the regulation of the axonal elongation orientation with high spatial fidelity. The basic concept of the optical control of axon guidance described here can be principally extended to other axon guidance receptors.

Chapter 4.

Optical regulation of the growth cone motility in living organisms

4.1 Introduction of *C. elegans*

C. elegans is a tiny transparent nematode worm, about 1 mm long in adult. It takes only 3–4 days to become adult from egg at 20 °C, containing multiple larvae stages from L1 to L4[100]. Although the number of cells in adult *C. elegans* is less than 1,000, the cellular or molecular biological processes during development have high similarity with that of other species, including human: about 70% of human genes have *C. elegans* homologues[101]. Since the pioneering work of Sydney Brenner[102], it has been an excellent genetic model organisms to identify key molecules responsible for various phenomena during the embryonic development.

One of the great advantages in using *C. elegans* as a model organisms is the ease of genetic manipulation[82]. A variety of mutagens, including ethane methylsulfonate, can easily induce genetic mutations and deletions. It contributes to the preparation of mutant worms and to the screening of mutants with specific phenotype, which will lead to the identification of important genes for biological events of interest.

Another important feature for the genetic manipulation in *C. elegans* is extrachromosomal array[103]. Upon microinjection of exogenous DNAs into gonad, the DNAs form a high-molecular-weight array mainly composed of tandem repeats of the co-injected sequence. The array is usually not incorporated in to the endogenous chromosomes, thus it is called “extrachromosomal” array. The key feature of the array is that it is heritable to about half of the progenies of injected worms despite the huge molecular size. To obtain a transgenic worm strain expressing exogenous genes in specific types of cells, we only have to co-inject multiple plasmid DNAs encoding the genes with its specific promoter into the worm.

With the help of the genetic techniques described above, various molecules involved in axon guidance have been analyzed and found to share common guidance mechanisms with other

species, including mammals. For example, homolog of DCC and netrin-1 have been identified in *C. elegans* as UNC-40 and UNC-6. UNC-6 is secreted from *C. elegans* ventral cells, which is necessary for the circumferential axon guidance (**Figure 4-1a**)[104]. AVM neuron, whose cell body located along the lateral body of the worm, expresses UNC-40[105]. Its axon is attracted by the UNC-6 gradients, extending to the ventral nerve cord. By contrast, VD neurons, whose cell body positioned at the ventral nerve cord, expresses UNC-40 but extends their axons dorsally[27]. It is because they also express UNC-5, another UNC-6 receptor which converts attractive signaling to repulsive one[106]. Mutagenesis screening also identified downstream molecules involved in the UNC-40 signaling, CED-10, UNC-115 and UNC-34, which are homologues of Rac, abLIM and Enabled, respectively (**Figure 4-1b**). Moreover, imaging analysis revealed that UNC-40 preferentially localized to the ventral side, which corresponds to the source of UNC-6[107]. It indicates that UNC-6 induced UNC-40 localization constitute a positive feedback loop to sense UNC-6 gradient, which might be the case in other species.

Optical transparency of *C. elegans* also serves to the investigation of nervous development *in vivo*. By careful microscopic observation of individual neurons, all 302 neuron lineages were traced and their connectivity were completely mapped[108]. Time lapse imaging of individual neurons labeled with fluorescent protein also contributed to the analysis of axon guidance procedures and growth cone behaviors during development[26, 106, 107]. As for HSN neuron, for instance, which is also guided by UNC-6 gradient (**Figure 4-1a**), the dynamic relationship between the site of growth cone formation and the UNC-6-induced localization of proteins was clarified. Moreover, morphological changes of HSN growth cones at each larvae stage were found to be associated with extracellular structures.

Because of the ease of genetic manipulation and the optical transparency, *C. elegans* is a suitable model organisms to study the mechanisms of axon guidance in living animals. In addition

to the fluorescent observation, using optogenetic tools to perturb intracellular signaling would be a powerful approach to dissect context-dependent cellular behaviors *in vivo*, which was already shown by ChR2 systems to clarify the role of individual neurons in specific *C. elegans* behaviors of interest[109]. For the above reasons, I selected *C. elegans* as a model organism to investigate it is possible to control the direction of axon extension with the photo-activating system of the axon guidance receptor in **Chapter 3**.

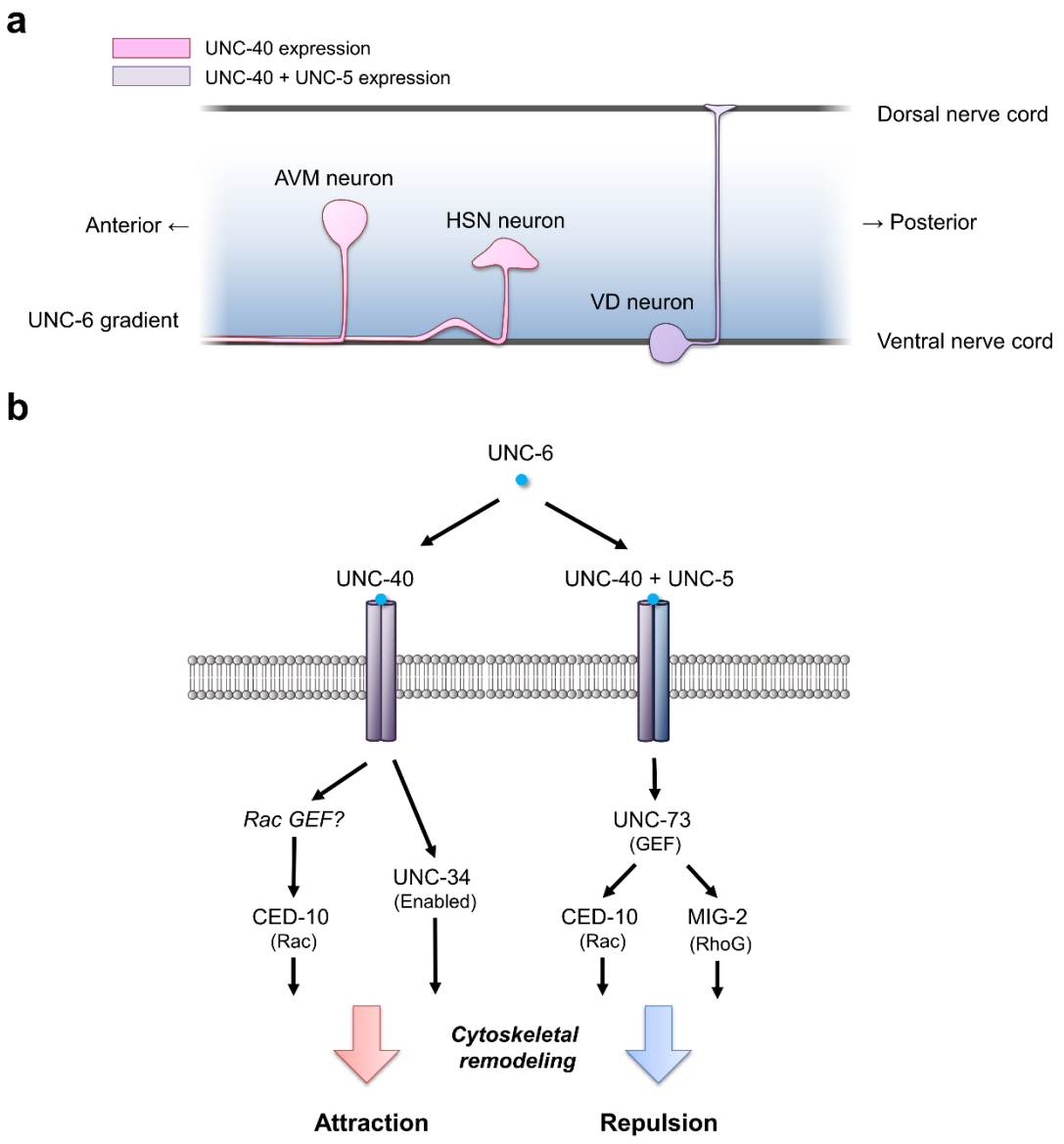

Figure 4-1. Axon guidance in *C. elegans*.

(**a**) Lateral view of *C. elegans* with circumferential neurons. Blue gradients indicate the UNC-6 gradient. Colors of neurons represent their receptor expression patterns indicated by the color boxes. (**b**) Mechanisms of axon guidance by UNC-6 via UNC-40 or UNC-40/UNC-5 hetero dimer.

4.2 Photo-attraction of the VD growth cones

Of several neuron types in *C. elegans*, GABAergic VD motor neurons are guided by UNC-6 in the post-embryonic stage. The behavior of their growth cones in the neural network establishment stage has been analyzed using time-lapse imaging[26, 110]. For these reasons, VD neurons in *C. elegans* were selected as a target for the *in vivo* photo-manipulation of the growth cone behavior.

Regarding the amino acid sequence in the intracellular domain, UNC-40, a *C. elegans* homolog of DCC, exhibits low homology to vertebrate DCC[111]. To improve the efficiency of light-induced signal transduction in *C. elegans* cells, DCC in PA-DCC was replaced with UNC-40, resulting in a protein named PA-UNC-40. In addition, the C-terminus of PA-UNC-40 was fused with a fluorescent protein, Venus for examining its expression (**Figure 4-3a**). The gene of PA-UNC-40::Venus was placed under the *unc-47* promoter for the expression in GABAergic neurons including VD neurons[88]. To improve the translation efficiency, *C. elegans* consensus sequence (AAAA) was introduced before the translation initiation site.

VD axons express both UNC-40 and UNC-5, which cooperates with UNC-40 to mediate repulsive response to UNC-6, thereby extending dorsally at the L2 stage[106, 110]. To eliminate interference with the endogenous guidance system in VD axons, a mutant worm lacking both *unc-5* and *unc-6* (JN1907 *unc-5(e53); unc-6(ev400)*) was generated by crossing JN1906 *unc-5(e53)* with NW434 *unc-6(ev400)* (**Figure 4-2b**). Subsequently, cDNAs of PA-UNC-40::Venus and mCherry were introduced into the mutant and a transgenic line was obtained (JN1900). The PA-UNC-40::Venus molecules distributed uniformly on the VD growth cone membrane (**Figure 4-3a** and **b**), which was similar to the localization pattern of UNC-40 in the *unc-6* null mutant background[107]. A transgenic line expressing only mCherry in VD axons was also generated

(JN1901). Consistent with the previous report[106], almost all VD axons failed to reach the dorsal nerve cord in the generated strain (**Figure 4-4a** and **b**). The PA-UNC-40 expression in the mutant did not rescue the axon guidance defects in VD axons (**Figure 4-4a** and **b**).

For the time lapse imaging of living *C. elegans*, the worms have to be immobilized by anesthetic regents. The selection of anesthetic reagents is important for the observation of axonal elongation in living worms. It is because some chemical compounds like NaN_3, a widely used anesthetizing molecule for *C. elegans*, prevent developmental processes[112]. Among the reagents, levamisole is a cholinergic agonist that binds specifically to the acetylcholine receptor, which is responsible for the muscle contraction[113]. Upon levamisole treatment, *C. elegans* fails to move properly and become immobilized. In this study, levamisole was selected to immobilize worms in the following experiments.

Growth cones of VD neurons in anesthetized L2 transgenic mutant worms with or without PA-UNC-40::Venus expression (JN1900 or JN1901) were visualized with fluorescence of mCherry. Before illumination, ruffling VD growth cones showed slow movement in different directions (0.90 ± 0.26 μm h^{-1}, $n = 10$). The slower moving velocity can be attributed to the deletion of *unc-5* and *unc-6*, which caused severe developmental retardation in all strains devoid of both genes (JN1900, JN1901, JN1902, and JN1907) (**Figure 4-2b**). A part of the growth cones was illuminated with blue laser light under the confocal microscope in a pulse-like manner (2 s min^{-1}). Time lapse imaging with light stimulation showed growth cone attraction toward the illuminated side (**Figure 4-5**). To ascertain the extent of light-induced attraction, centroids of each illuminated growth cone were plotted over time (**Figure 4-6** and **Figure 4-7**). The centroids with a positive value represent growth cone attraction toward the illuminated side. The temporal profile of centroid plots revealed clear light-induced attraction in growth cones expressing PA-UNC-40::Venus, while light illumination itself did not affect the growth cone movements without PA-

UNC-40::Venus expression. The light-induced attraction was observed especially 15 min after the onset of the illumination, judging from the 98% confidence interval (0.02–0.14 μm).

After repeated illuminations to the growth cones, a PA-UNC-40::Venus localization pattern changed from a uniform distribution to preferential localization to the illuminated side of the all examined growth cones (**Figure 4-3a** and **b**). The localization pattern of PA-UNC-40::Venus after repeated illuminations were similar to the ventral localization of UNC-40 corresponding to the endogenous UNC-6 gradient generated by ventral cells[107]. The change in the localization pattern of PA-UNC-40 suggests that light-induced activation of PA-UNC-40 corresponds to the intrinsic property of UNC-40 activation by UNC-6. To further confirm that photo-attraction with PA-UNC-40 is due to the activation of UNC-40, *ced-10*, a downstream molecule of UNC-40 signaling[105, 114] was deleted from JN1900 by crossing with MT5013 *unc-5(e53)*, named JN1902 (**Figure 4-2**). The light-induced attraction was abolished in the mutant, which suggests that photo-attraction with PA-UNC-40 involves activation of UNC-40 signaling (**Figure 4-5** and **Figure 4-7**). Collectively, blue laser light illumination enables attraction of the growth cone in living nematode worms.

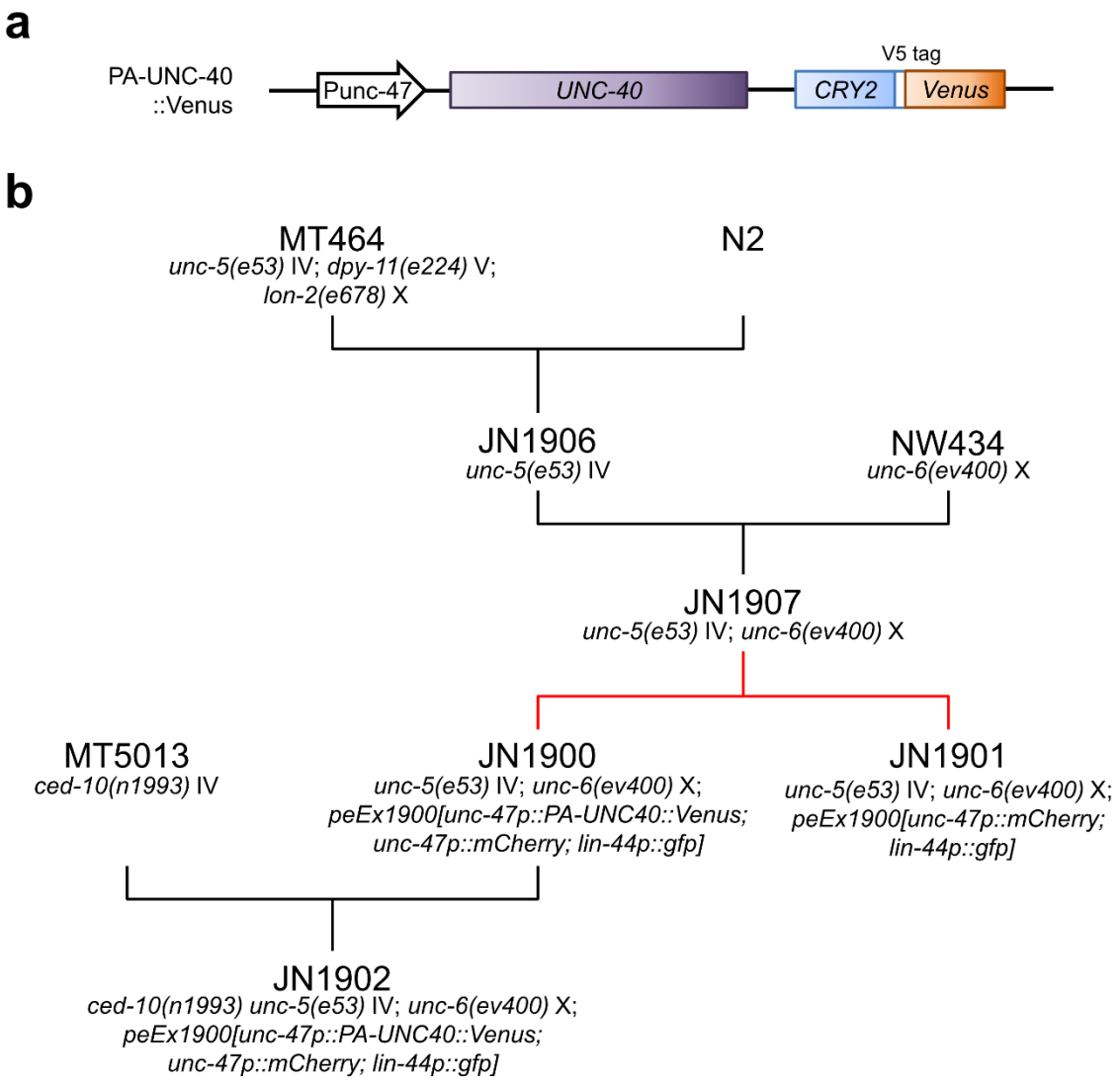

Figure 4-2. Materials for experiments in *C. elegans.*

(**a**) Domain structure of PA-UNC-40 molecule. All text in italics refers to the genes of their corresponding proteins. Punc-47 represents a promoter for gene expression. UNC-40 is connected with CRY2 via GS linker (GGRGGGGSGGGGS). Venus is a yellow fluorescent protein whose sequence is optimized for *C. elegans* expression. White square shows epitope V5 tag. (**b**) *C.elegans* strains used in this study. N2 is wild-type worm strain. Each strain is shown by its name, followed by its information about alleles and transgenes. Black lines show the mating pares. Red lines show the generation of transgenic lines by plasmid injections.

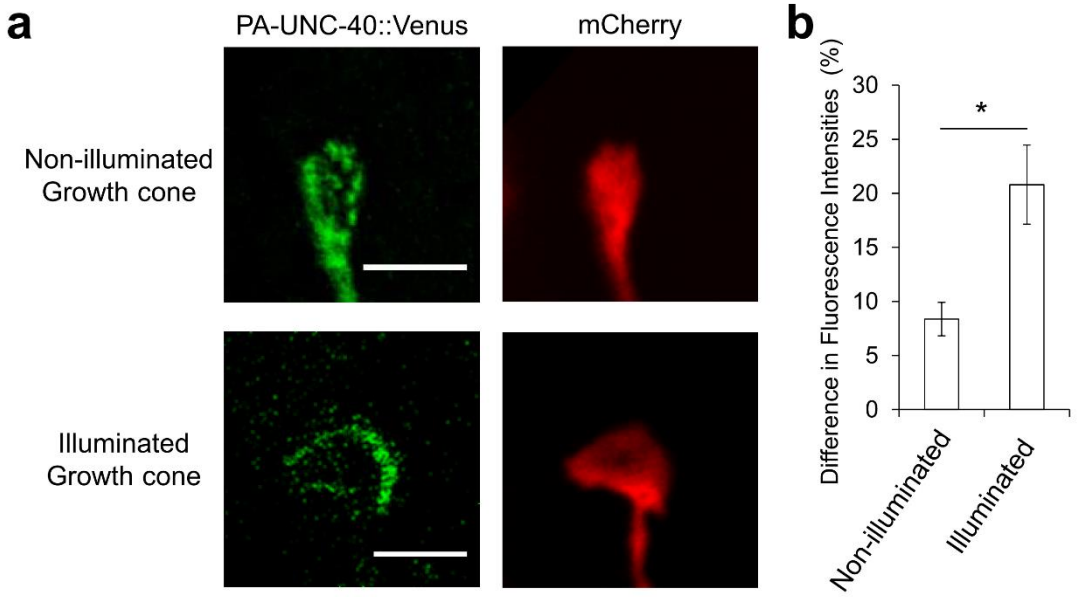

Figure 4-3. Localization of PA-UNC-40 molecule in VD growth cones.

(**a**) Fluorescence images of *unc-5(e53); unc-6(ev400)* VD growth cones expressing PA-UNC-40::Venus and mCherry. Lower images were taken after the illumination to the right side of the growth cone (2 s min^{-1} pulses for 30 min). Scale bar, 3 μm. (**b**) Analysis of the PA-UNC-40::Venus distribution on the growth cone. The difference in fluorescence intensities was defined as the difference of the total Venus fluorescence intensities in each side relative to the total Venus intensity in the both side. Then, the obtained result was normalized by that of mCherry fluorescence. Mean distribution inequities were shown as scores. Error bars, s.e.m (n = 5). *P < 0.05, unpaired t-test.

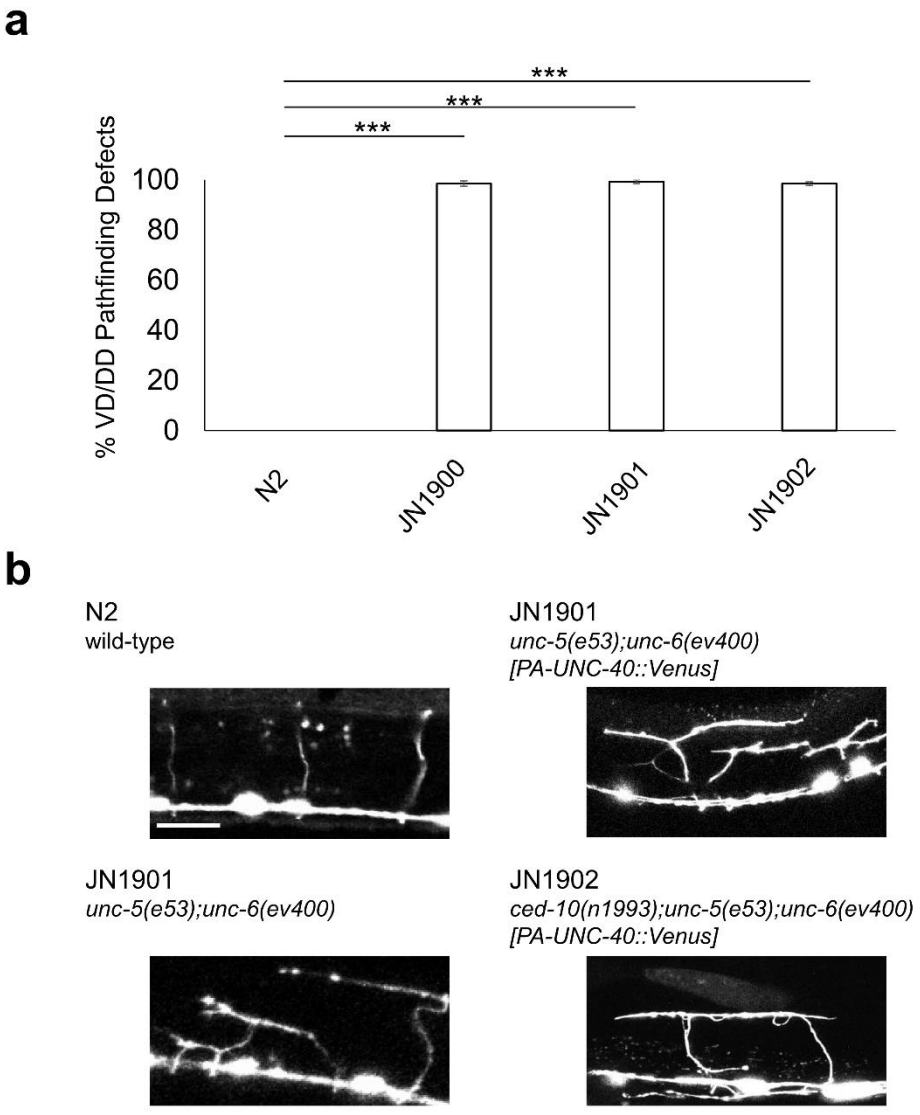

Figure 4-4. Axon guidance defects of worms used for this study.

(**a**) Percentage of VD/DD axon pathfinding defects. Statistical significance was determined by one-way ANOVA followed by Dunnett's test for multiple comparison, ***$P < 0.005$. Error bars, SEM ($n > 100$). (**b**) Fluorescence micrographs of L4 worms showing VD/DD axons. Scale bar, 20 μm.

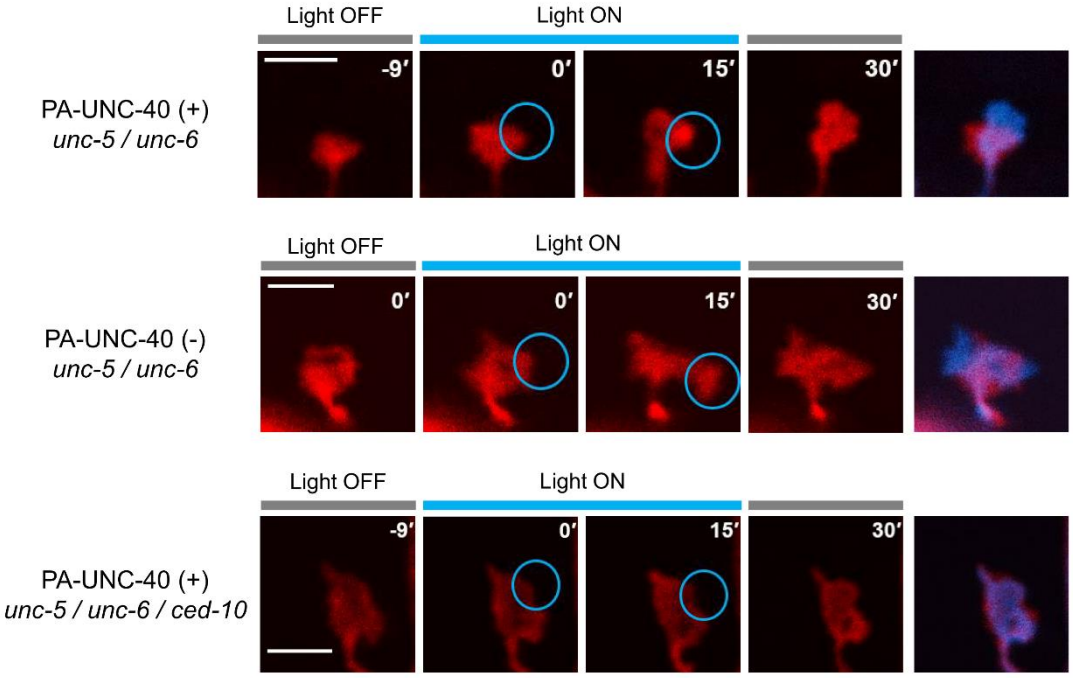

Figure 4-5. Light-induced growth cone attraction in *C. elegans* expressing PA-UNC-40.
Time lapse images showing the movements of illuminated VD growth cones. Anesthetized L2 worm with or without PA-UNC-40::Venus were observed with the mCherry fluorescence. Illuminated regions with blue laser light (2 s min^{-1} pulses, 488 nm) were represented as blue circles. The merged images from different time points (Red; 0 min, Blue; 30 min) were attached at the end of the images. Scale bar, 3 μm.

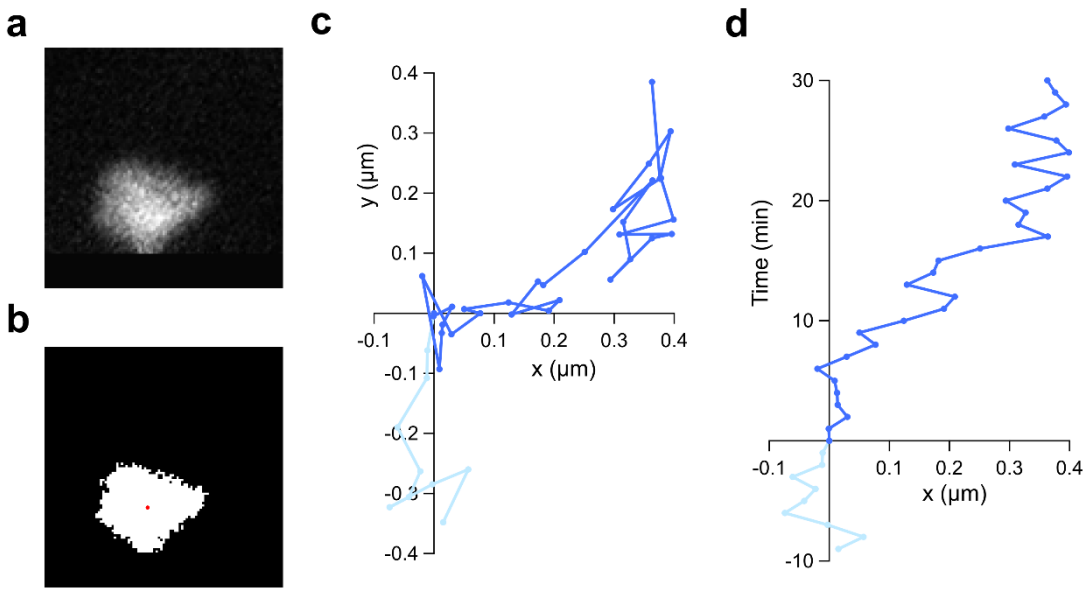

Figure 4-6. Procedures for growth cone centroid analysis in *C. elegans* VD neurons.

(**a**) Representative image of the trimmed growth cone in Figure 4-5a. The trimmed growth cone was rotated and inverted to put the illuminated side at the right and the axon at the bottom. (b) Binarized image of Figure 4-6a. The red dot indicates the position of the centroid. (c) Centroid plots of the growth cone in a and b. The position of centroid at 0 min was defined as the origin. (d) Centroids plots against time modified from c. The centroid displacement from the origin along x-axis (Fig. S7c) was displayed against time-axis.

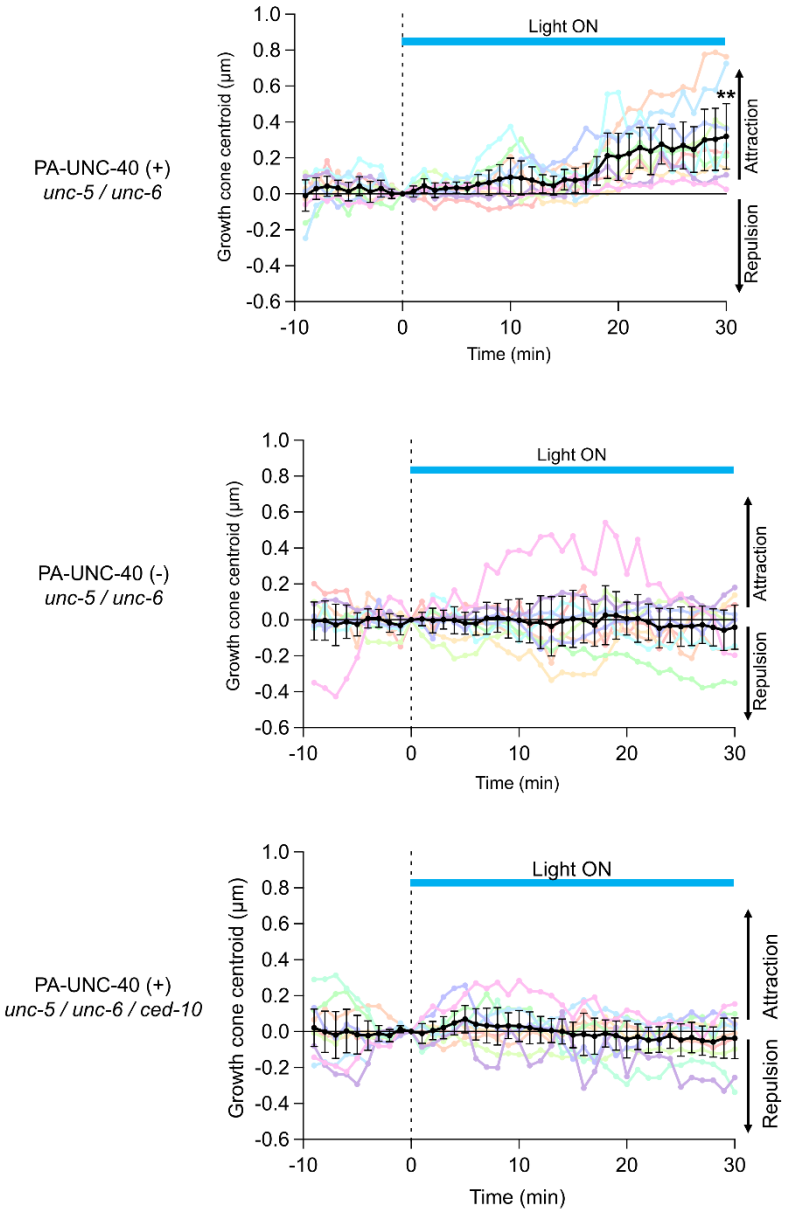

Figure 4-7. Temporal centroid plots of periodically illuminated growth cones.

Worm strains used in these experiments were *unc-5(e53); unc-6(ev400)* with or without PA-UNC-40::Venus expression. Each data is represented by a colored line. Averaged data are shown as black. Blue bars indicate the illumination periods. Error bars, 98% CI of the mean ($n = 10$). $^{**}P < 0.01$ versus PA-UNC-40 (-) *unc-5 / unc-6* at 30 min, unpaired *t*-test.

4.3 Analysis of growth cone motility with photo-attraction system

A heterogeneous extracellular milieu exists around the growth cone in *C. elegans*. During the extension of VD neurons in L2 stage, VD growth cones stall at two physical barriers, the lateral nerve cord, and the dorsal body wall muscle (**Figure 4-8**)[26]. Stalled growth cones spread along the barrier and become anvil-shaped. The anvil-shaped VD growth cones were trapped in these structures for from tens of minutes to several hours, then resumes dorsal extension and finally reaches dorsal nerve cord.

To examine the motility difference among directions, the anvil-shaped VD growth cone, which is presumably trapped at the lateral nerve cord, was sequentially illuminated on two sides during the observation (**Figure 4-9a** and **b**). First, the dorsal side of the anvil-shaped VD growth cone was illuminated. The blue light did not induce any visible attractive response. In contrast, the subsequent anterior illumination triggered marked growth cone intrusion into the illuminated area. These behaviors were visualized by centroid tracking from multiple experiments, showing no readily observable dorsal movement (0–30 min), but a gradual shift to the illuminated side along the anterior-posterior axis (30–60 min) (**Figure 4-9c**). Judging from the 98% confidence intervals, the examined growth cones were attracted to the illuminated side especially 13 min after the onset of the illumination (0.01–0.59 μm). It is noteworthy that centroid plots with a positive value represent attraction to the illuminated side. As described above, illumination to the anvil-shaped VD growth cone evoked either attractive or non-attractive response, depending on the illumination position. These results demonstrate that the PA-UNC-40 system enables analysis of the growth cone behavior within intrinsic extracellular environments by photo-manipulation *in vivo*.

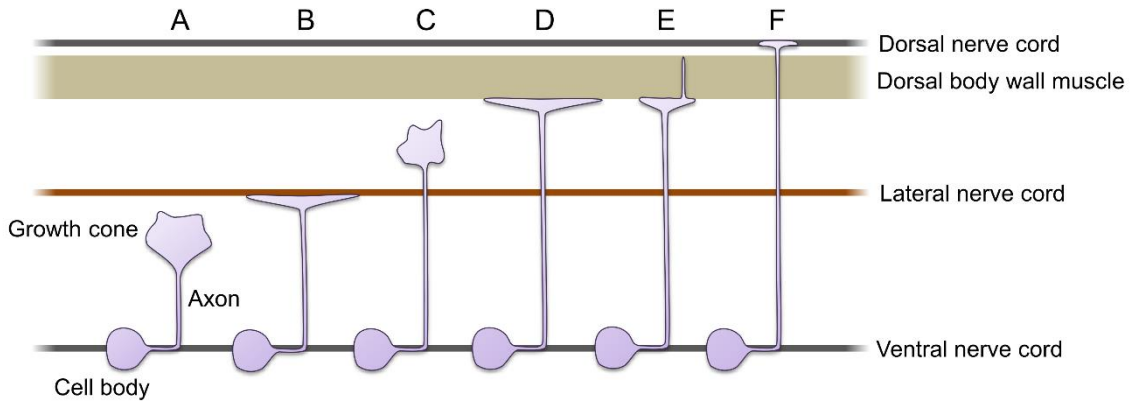

Figure 4-8. Schematics of VD growth cone behaviors during dorsal migration.

The X-axis represents time. Round-shaped VD growth cones initiate dorsal migration from the cell body on the ventral nerve cord (A). Growth cones become anvil-shaped at the lateral nerve cord and stalled for several tens of minutes (B). Growth cones resume dorsal migration across the epidermis (C). Growth cones become anvil-shaped at the dorsal body wall muscle and stalled for several hours (D). Anvil-shaped VD growth cones extends finger-like structures across the muscle (E). The VD axons reach the dorsal nerve cord and the growth cones collapse.

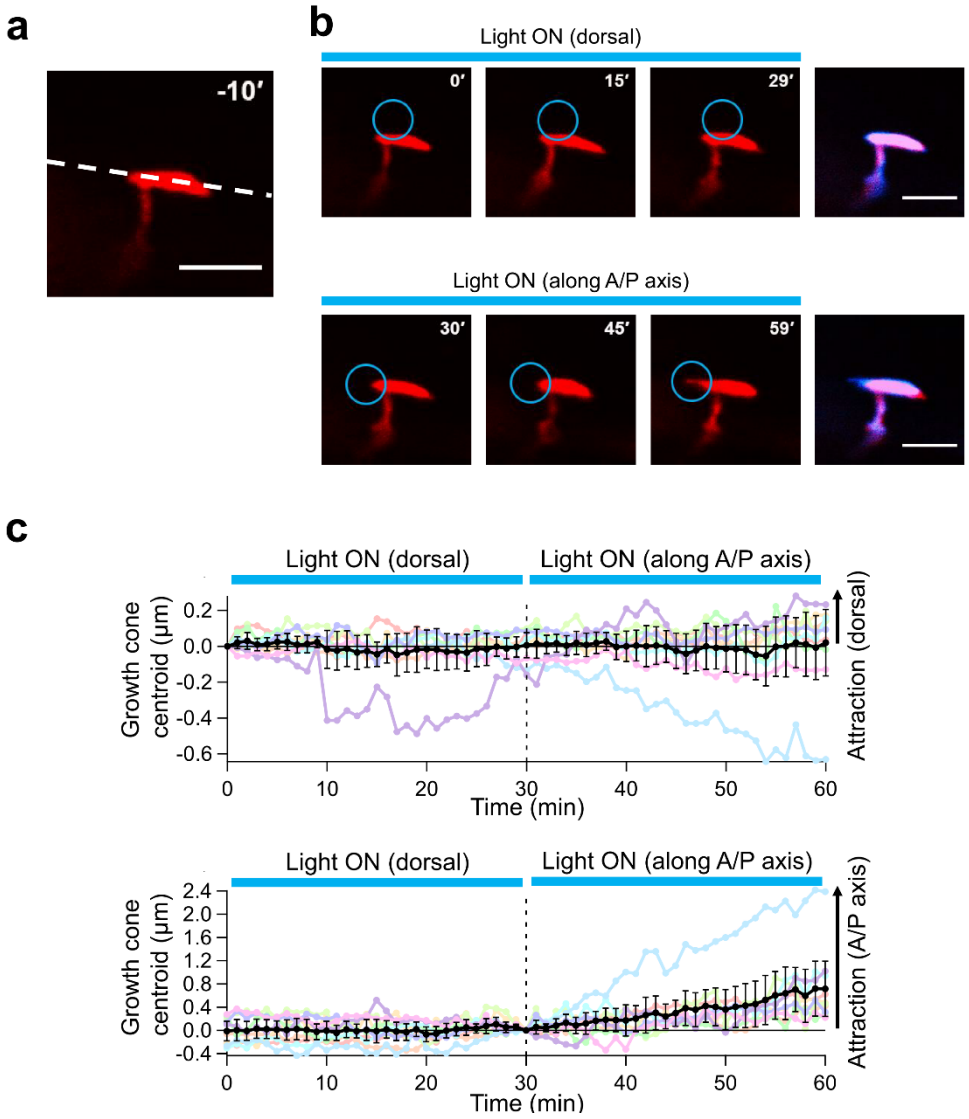

Figure 4-9. Photo-manipulation of anvil-shaped VD growth cones' motility.

(**a**) A fluorescence image of an anvil-shaped VD growth cone. Ventral is down and anterior is to the left. White dotted line represents the putative lateral nerve cord. Scale bar, 3 μm. (**b**) Partial illumination of the anvil-shaped VD growth cone. First, blue light (2 s min^{-1} pulses, 488 nm) was exposed to the dorsal side (0–29 min). Subsequently, the anterior side was illuminated (30–59 min). The merged image from different time points (upper image: Red; 0 min, Blue; 30 min, lower image: Red; 0 min, Blue; 60 min) was attached at the end of the images. Scale bar, 3 μm. (**c**) Temporal centroid plots of the illuminated anvil-shaped VD growth cones. Second illuminations were performed on either side of the growth cones along the anterior-posterior axis. Each experimental trial is shown with the same colored line. Averaged data are shown as black. Blue bar indicate the illumination periods. Error bars, 98% CI of the mean (n = 10).

4.4 Discussion

I established transgenic worms expressing PA-UNC-40 in GABAergic VD motor neurons. Blue laser scanning on a part of growth cones attracted them to the illuminated side in anesthetized developing larvae. The photo-attraction system revealed that VD growth cones trapped by lateral nerve cord have an anisotropic motility: the motility was restricted to the orientation of the nerve cord. The results demonstrate that it enables direct analysis of the growth cone behavior within heterogeneous extracellular environments in living organisms.

Photo-attraction with PA-UNC-40 was completely abolished in *ced-10* lacking mutant. The result suggests that *C. elegans* UNC-40 was activated with the same light-induced receptor oligomerization system as in PA-DCC. Although the amino acids sequence of UNC-40 has a low similarity with DCC in the intracellular domain, the results constitute direct evidence showing that a common activation mechanism exists in DCC homologs among species.

As discussed in **Chapter 3**, optical modulation of biological phenomena sometimes suffers from the adverse effects of the light itself. Besides the photo-thermal effects, photo-toxicity is also critical in living organisms. In earlier observations using a confocal laser microscopic system, for instance, slowed migration of growth cones in *C. elegans* was detected with excessive light exposure[26]. I also observed axon retraction in my developed system with intentionally longer illumination time than the standard protocol described, especially in the *C. elegans* growth cone (data not shown), which suggests the susceptibility of the mutant *C. elegans* growth cones to light-induced damage. Nevertheless, the photo-toxic effect is avoidable by optimizing the illumination protocol because I rarely observed axon retraction or slowed migration during the assays in the established illumination condition. To maximize the light-induced attractive response, it is important to seek the best light condition which enables both effective photo-activation and

reduced light-adverse effects. Such a condition can be achieved by changing the exposure time, intensity interval, and the illumination position with careful consideration of the adverse effects.

One benefit of my strategy is its applicability to an *in vivo* system, enabling the analysis of growth cone behavior in living animals. I demonstrated that light illumination can attract the VD growth cone expressing PA-UNC-40 in living worms. It is particularly interesting that the dorsal side illumination to the anvil-shaped VD growth cone did not induce attractive response. The shape and position of the illuminated growth cone[26] suggested that the light-induced attractive signaling with PA-UNC-40 was insufficient to cross the lateral nerve cord where the dorsal movement of the growth cone was physically hampered. Given that the extent of light-induced downstream signaling was not different in illuminations on either side, the lateral cord was able to impede the VD growth cone advancement physically, thereby restricting its motility.

Regarding the onset of the photo-attraction, judging from the 98% confidence intervals, there was no significant difference between round-shaped (15 min) and anvil-shaped (13 min). However, the shape of the averaged trajectories might be different. The difference, if any, can be explained by the following fact: the anvil-shaped VD growth cones were trapped in putatively adhesive lateral nerve cords, although round-shaped growth cones were not surrounded by such extracellular structures. Taking that fact into account, the difference in the centroids movement between two cases is explainable using the existence of the extracellular structures along the direction of the movement.

As demonstrated here, the developed photo-manipulation system can analyze the growth cone behavior in the presence of surrounding physical barriers in living animals. The possibility exists that it will further enable us to examine other types of growth cones to reveal other unknown motility regulation by extracellular structures during the nervous development. Moreover, as shown in **Chapter 3**, the developed optical system to control axon guidance receptors can analyze

the modulation of intracellular signaling by extracellular matrix. Further analysis of those interactions between growth cones and surrounding environments will contribute to the precise understanding of the axon pathfinding *in vivo*, which is crucial for curing various nervous disorders.

4.5 Conclusion

In summary, I confirmed the applicability of the optical system to attract growth cone in living worms by activating *C. elegans* UNC-40, a homolog of vertebrate DCC, with light-induced oligomerizing module. The developed photo-manipulation system can analyze the growth cone behavior in the presence of surrounding physical barriers in living animals. The possibility exists that the system will further enable us to examine, in a site-specific manner, how extracellular environments permit or inhibit growth cone entry to achieve highly precise neural wiring in a specific stage of the development.

Chapter 5.

General Conclusion

Axon guidance is a fundamental step in nervous development to connect correct synaptic partners among a vast number of neurons. Axons are guided by molecular interactions between extracellular guidance cue ligands and their receptors on their growth cones. Although the molecular mechanisms of the ligand–receptor signaling have been intensively investigated in *in vitro* experiments, how they are modulated by surrounding complicated extracellular environments in living animals is not fully understood because of the lack of tools. To address the issue, I developed an optical system to control the orientation of neurite outgrowth by activating axon guidance receptor DCC with light-induced protein oligomerization system. The elongating axon was attracted by light with the developed system, both *in vitro* and *in vivo*.

In **Chapter 3**, I described an optical system to activate DCC with light-induced oligomerization system. Upon light illumination, DCC transiently reversibly oligomer and the downstream signaling was transiently activated. In cultured chick DRG neurons, the locally photo-activated DCC induced asymmetric activation of the downstream signaling within the illuminated growth cones, changing the direction of extending axons to the illuminated side. It was also demonstrated that the axonal photo-attraction with the system is repeatable, which ensures the achievement of high spatial fidelity in the regulation of the axonal elongation orientation. Moreover, extracellular-matrix-dependent modulation of the guidance signaling was also observed, which indicates the potential of the optical system in the analysis of the modulation of axon guidance signaling by heterogeneous extracellular matrix in living tissue.

In **Chapter 4**, I applied the developed axonal photo-attraction system to nematode worm *C. elegans*. Transgenic *C. elegans* stably expressing photo-activatable UNC-40, a homolog of DCC, was generated. Laser illumination to a part of growth cones in living anesthetized worms attracted growth cones to the illuminated side. Mutant experiments supported that the photo-attraction was due to the activation of UNC-40 with light. It was also demonstrated that the developed photo-

manipulation system was able to analyze the growth cone behaviors within the extracellular structures in living animals and revealed that the motility of VD growth cones was restricted to the orientation of the lateral nerve cord. These results indicate the potential of the developed optical system that it enables the direct analysis of the modulation of various growth cone behaviors by extracellular structures in living organisms.

As a future perspective of this research, there would be mainly three promising advancement. First, it is possible to expand the developed optical system for photo-activating other guidance receptors with similar activation mechanisms. With the development of red-shifted light-oligomerization system, the multiple modulation of different axon guidance receptors will reveal the dynamics of combinatorial signaling effects on the growth cone behavior in living animals. Second, the system has a potential to analyze the modulation of axon guidance by extracellular matrix and structures in living tissue. The analysis of the environmental modulation of the growth cone behaviors will unveil the mechanisms of the precise neural wiring in the nervous development, thereby leading to the steep understanding of the mechanism of various nervous disorders. Third, further optimization of the illumination protocol and the photo-activating system will enable artificial wiring of the developing neurons. It would become a novel approach in the regenerative therapies for the nervous disorders with disrupted neural connections.

Taken altogether, DCC connected with CRY2 is activatable with blue-light illumination by the photo-oligomerization of fused CRY2. Results show that the local activation within growth cones changed the direction of the growth in both chick DRG neuron and *C. elegans* VD neuron. This is the first method that enables optical manipulation of growth cone behavior *in vivo*. The system is readily applicable to other guidance receptors, thereby expanding the range of experimental tools to analyze the guidance mechanisms, particularly in the developing nervous system. The photo-manipulation system can analyze the modulation of growth cone behaviors by

extracellular matrix and structures. Further optimization of the photo-manipulation system will enable the optical wiring of the neurons in living animals, which can contribute considerably to the development of regenerative therapies for neurodegenerative disorders.

Acknowledgement

The present thesis was completed under the supervision of Prof. Takeaki Ozawa. I would like to express my sincere appreciations for his constant support, guidance, and encouragement to complete my research throughout the study. I appreciated all the stuff members in Prof. Ozawa lab., especially Dr. Mitsuru Hattori, Dr. Hideaki Yoshimura, and Dr. Rintaro Shimada for a number of stimulating discussions and their critical comments on my research. Also, I have greatly benefited from well talented other graduate students in Prof. Ozawa lab., who gave a lot of intuitive suggestions and precious peer pressure. Without the environmental advantages, I would not maintain the high level of motivation for science, which enables me to work hard throughout my research.

The experiments in cultured chick DRG neurons part in Chapter 3 was heavily supported by Prof. Hiroyuki Kamiguchi lab., especially by Dr. Tomonobu Hida. I had a great opportunity to learn to dissect DRG neurons from chick embryos. I would like to express my sincere appreciations for their time devotion for critically reading the manuscript. Without their kind supports, this thesis would not be completed.

The experiments in transgenic *C. elegans* part in Chapter 4 was heavily supported by Prof. Yuichi Iino lab., especially by Dr. Hayao Ohno and Mr. Hiroshi Toriyabe. I would like to express my sincere appreciations for their time devotion for establishing a variety of mutants and transgenic lines and for critically reading the manuscript. Without their kind supports, this thesis would not be completed.

I thanks Advanced Leading Graduate Course for Photon Science (ALPS) and JSPS Research Fellowship for Young Scientists for their financial supports and overseas experience.

Especially in ALPS program, I deeply appreciated Prof. Michael White and Dr. Shane Herbert in the University of Manchester for hosting me in U.K. and Prof. Hideo Higuchi for his encouragement as a secondary supervisor throughout my Ph.D. course.

Finally, I gave great thanks to my family for giving me this great opportunity to study in the University of Tokyo and also for encouraging me to do what I truly love to do. I cherish all the priceless experiences in Prof. Ozawa lab. in the University of Tokyo.

Reference

1. Li X. G., Somogyi P., Ylinen A., Buzsáki G. The hippocampal CA3 network: An *in vivo* intracellular labeling study. *The Journal of Comparative Neurology* **339**, 181–208 (1994).

2. Azevedo F. A. C. *et al.* Equal numbers of neuronal and nonneuronal cells make the human brain an isometrically scaled-up primate brain. *The Journal of Comparative Neurology* **513**, 532–541 (2009).

3. Rogers S. L., Letourneau P. C., Palm S. L., McCarthy J., Furcht L. T. Neurite extension by peripheral and central nervous system neurons in response to substratum-bound fibronectin and laminin. *Dev. Biol.* **98**, 212–220 (1983).

4. Greene N. D. E., Copp A. J. Development of the vertebrate central nervous system: Formation of the neural tube. *Prenat. Diagn.* **29**, 303–311 (2009).

5. Huang X., Saint-Jeannet J.-P. Induction of the neural crest and the opportunities of life on the edge. *Dev. Biol.* **275**, 1–11 (2004).

6. Debanne D., Campanac E., Bialowas A., Carlier E., Alcaraz G. Axon physiology. *Physiol. Rev.* **91**, 555–602 (2011).

7. Geraldo S., Gordon-Weeks P. R. Cytoskeletal dynamics in growth-cone steering. *J. Cell Sci.* **122**, 3595–3604 (2009).

8. Tessier-Lavigne M., Goodman C. S. The molecular biology of axon guidance. *Science* **274**, 1123–1133 (1996).

9. Dickson B. J. Molecular mechanisms of axon guidance. *Science* **298**, 1959–1964 (2002).

10. Nogi T. *et al.* Structural basis for semaphorin signalling through the plexin receptor. *Nature* **467**, 1123–1127 (2010).

11. Finci Lorenzo I. *et al.* The crystal structure of netrin-1 in complex with DCC reveals the bifunctionality of netrin-1 as a guidance cue. *Neuron* **83**, 839–849 (2014).

12. Stein E., Tessier-Lavigne M. Hierarchical organization of guidance receptors: Silencing of netrin attraction by Slit through a Robo/DCC receptor complex. *Science* **291**, 1928–1938 (2001).

13. Yu T. W., Bargmann C. I. Dynamic regulation of axon guidance. *Nat. Neurosci.* **4**, 1169–1176 (2001).

14. Hall A., Lalli G. Rho and Ras GTPases in axon growth, guidance, and branching. *Cold Spring Harb. Perspect. Biol.* **2**, a001818 (2010).

15. Robles E., Gomez T. M. Focal adhesion kinase signaling at sites of integrin-mediated adhesion controls axon pathfinding. *Nat. Neurosci.* **9**, 1274–1283 (2006).

16. Mitra S. K., Hanson D. A., Schlaepfer D. D. Focal adhesion kinase: In command and control of cell motility. *Nature Reviews Molecular Cell Biology* **6**, 56–68 (2005).

17. Moore S. W., Zhang X., Lynch C. D., Sheetz M. P. Netrin-1 attracts axons through FAK-dependent mechanotransduction. *J. Neurosci.* **32**, 11574–11585 (2012).

18. Tojima T. *et al.* Attractive axon guidance involves asymmetric membrane transport and exocytosis in the growth cone. *Nat. Neurosci.* **10**, 58–66 (2007).

19. Sutherland D. J., Pujic Z., Goodhill G. J. Calcium signaling in axon guidance. *Trends Neurosci.* **37**, 424–432 (2014).

20. Ming G.-l. *et al.* cAMP-dependent growth cone guidance by netrin-1. *Neuron* **19**, 1225–1235 (1997).

21. Lohof A., Quillan M., Dan Y., Poo M. Asymmetric modulation of cytosolic cAMP activity induces growth cone turning. *J. Neurosci.* **12**, 1253–1261 (1992).

22. Tojima T., Itofusa R., Kamiguchi H. The nitric oxide–cGMP pathway controls the directional polarity of growth cone guidance via modulating cytosolic Ca^{2+} signals. *J. Neurosci.* **29**, 7886–7897 (2009).

23. Nishiyama M. *et al.* Cyclic AMP/GMP-dependent modulation of Ca^{2+} channels sets the polarity of nerve growth-cone turning. *Nature* **423**, 990–995 (2003).

24. Xiang Y. *et al.* Nerve growth cone guidance mediated by G protein-coupled receptors. *Nat. Neurosci.* **5**, 843–848 (2002).

25. Fraher J. P., Dockery P., O'Donoghue O., Riedewald B., O'Leary D. Initial motor axon outgrowth from the developing central nervous system. *J. Anat.* **211**, 600–611 (2007).

26. Knobel K. M., Jorgensen E. M., Bastiani M. J. Growth cones stall and collapse during axon outgrowth in *Caenorhabditis elegans*. *Development* **126**, 4489–4498 (1999).

27. McIntire S. L., Garriga G., White J., Jacobson D., Robert Horvitz H. Genes necessary for directed axonal elongation or fasciculation in *C. elegans*. *Neuron* **8**, 307–322 (1992).

28. Ebendal T., Jacobson C. O. Tissue explants affecting extension and orientation of axons in cultured chick embryo ganglia. *Exp. Cell Res.* **105**, 379–387 (1977).

29. Dazert S. *et al.* Focal delivery of fibroblast growth factor-1 by transfected cells induces spiral ganglion neurite targeting in vitro. *J. Cell. Physiol.* **177**, 123–129 (1998).

30. Serafini T. *et al.* The netrins define a family of axon outgrowth-promoting proteins homologous to *C. elegans* UNC-6. *Cell* **78**, 409–424 (1994).

31. Messersmith E. K. *et al.* Sernaphorin III can function as a selective chemorepellent to pattern sensory projections in the spinal cord. *Neuron* **14**, 949–959 (1995).

32. Ibáñez C. F., Ebendal T., Persson H. Chimeric molecules with multiple neurotrophic activities reveal structural elements determining the specificities of NGF and BDNF. *The EMBO Journal* **10**, 2105–2110 (1991).

33. Lumsden A. G. S., Davies A. M. Earliest sensory nerve fibres are guided to peripheral targets by attractants other than nerve growth factor. *Nature* **306**, 786–788 (1983).

34. Mortimer D. *et al.* Axon guidance by growth-rate modulation. *Proc. Natl. Acad. Sci. U. S. A.* **107**, 5202–5207 (2010).

35. Yuan X.-b. *et al.* Signalling and crosstalk of Rho GTPases in mediating axon guidance. *Nat. Cell Biol.* **5**, 38–45 (2003).

36. Gomez T. M., Spitzer N. C. *In vivo* regulation of axon extension and pathfinding by growth-cone calcium transients. *Nature* **397**, 350–355 (1999).

37. Gorbunova Y. V., Spitzer N. C. Dynamic interactions of cyclic AMP transients and spontaneous Ca^{2+} spikes. *Nature* **418**, 93–96 (2002).

38. Jacob S. N. *et al.* Signaling microdomains regulate inositol 1,4,5-trisphosphate-mediated intracellular calcium transients in cultured neurons. *J. Neurosci.* **25**, 2853–2864 (2005).

39. Aoki K., Nakamura T., Matsuda M. Spatio-temporal regulation of Rac1 and Cdc42 activity during nerve growth factor-induced neurite outgrowth in PC12 cells. *J. Biol. Chem.* **279**, 713–719 (2004).

40. Deisseroth K. Optogenetics. *Nat. Methods* **8**, 26–29 (2011).

41. Hausser M. Optogenetics: The age of light. *Nat. Methods* **11**, 1012–1014 (2014).

42. Airan R. D., Thompson K. R., Fenno L. E., Bernstein H., Deisseroth K. Temporally precise *in vivo* control of intracellular signalling. *Nature* **458**, 1025–1029 (2009).

43. Bruegmann T. *et al.* Optogenetic control of heart muscle *in vitro* and *in vivo*. *Nat. Methods* **7**, 897–900 (2010).

44. Leifer A. M., Fang-Yen C., Gershow M., Alkema M. J., Samuel A. D. T. Optogenetic manipulation of neural activity in freely moving *Caenorhabditis elegans*. *Nat. Methods* **8**, 147–152 (2011).

45. Toettcher J. E., Gong D., Lim W. A., Weiner O. D. Light-based feedback for controlling intracellular signaling dynamics. *Nat. Methods* **8**, 837–839 (2011).

46. Williams J. C. *et al.* Computational optogenetics: Empirically-derived voltage- and light-sensitive Channelrhodopsin-2 model. *PLoS Comput. Biol.* **9**, e1003220 (2013).

47. Katsura Y. *et al.* An optogenetic system for interrogating the temporal dynamics of Akt. *Sci. Rep.* **5**, 14589 (2015).

48. Illis L. S. Central nervous system regeneration does not occur. *Spinal Cord* **50**, 259–263 (2012).

49. Alexander G. E., Crutcher M. D. Functional architecture of basal ganglia circuits: Neural substrates of parallel processing. *Trends Neurosci.* **13**, 266–271 (1990).

50. Albin R. L., Young A. B., Penney J. B. The functional anatomy of basal ganglia disorders. *Trends Neurosci.* **12**, 366–375 (1989).

51. Lindvall O., Kokaia Z. Stem cells for the treatment of neurological disorders. *Nature* **441**, 1094–1096 (2006).

52. Bjorklund A., Lindvall O. Cell replacement therapies for central nervous system disorders. *Nat. Neurosci.* **3**, 537–544 (2000).

53. Politis M., Lindvall O. Clinical application of stem cell therapy in Parkinson's disease. *BMC Med.* **10**, 1 (2012).

54. Matsui T., Akamatsu W., Nakamura M., Okano H. Regeneration of the damaged central nervous system through reprogramming technology: Basic concepts and potential application for cell replacement therapy. *Exp. Neurol.* **260**, 12–18 (2014).

55. Martínez-Morales P. L. *et al.* Progress in stem cell therapy for major human neurological disorders. *Stem Cell Reviews and Reports* **9**, 685–699 (2013).

56. Pujic Z., Giacomantonio C. E., Unni D., Rosoff W. J., Goodhill G. J. Analysis of the growth cone turning assay for studying axon guidance. *J. Neurosci. Methods* **170**, 220–228 (2008).

57. Roy J., Kennedy T. E., Costantino S. Engineered cell culture substrates for axon guidance studies: Moving beyond proof of concept. *Lab on a Chip* **13**, 498–508 (2013).

58. Luo Y., Shoichet M. S. A photolabile hydrogel for guided three-dimensional cell growth and migration. *Nature Materials* **3**, 249–253 (2004).

59. Müller K., Naumann S., Weber W., Zurbriggen Matias D. Optogenetics for gene expression in mammalian cells. *Biol. Chem. Hoppe Seyler* **396**, 145–152 (2015).

60. Szobota S., Isacoff E. Y. Optical control of neuronal activity. *Annual Review of Biophysics* **39**, 329–348 (2010).

61. Wu Y. I. *et al.* A genetically encoded photoactivatable rac controls the motility of living cells. *Nature* **461**, 104–108 (2009).

62. Möglich A., Yang X., Ayers R. A., Moffat K. Structure and function of plant photoreceptors. *Annu. Rev. Plant Biol.* **61**, 21–47 (2010).

63. Shcherbakova D. M., Shemetov A. A., Kaberniuk A. A., Verkhusha V. V. Natural photoreceptors as a source of fluorescent proteins, biosensors, and optogenetic tools. *Annu. Rev. Biochem.* **84**, 519–550 (2015).

64. Yizhar O., Fenno Lief E., Davidson Thomas J., Mogri M., Deisseroth K. Optogenetics in neural systems. *Neuron* **71**, 9–34 (2011).

65. Zhang K., Cui B. Optogenetic control of intracellular signaling pathways. *Trends Biotechnol.* **33**, 92–100 (2015).

66. Bugaj L. J., Choksi A. T., Mesuda C. K., Kane R. S., Schaffer D. V. Optogenetic protein clustering and signaling activation in mammalian cells. *Nat. Methods* **10**, 249–252 (2013).

67. Chang K.-Y. *et al.* Light-inducible receptor tyrosine kinases that regulate neurotrophin signalling. *Nat. Commun.* **5**, ncomms5057 (2014).

68. Taslimi A. *et al.* An optimized optogenetic clustering tool for probing protein interaction and function. *Nat. Commun.* **5**, ncomms5925 (2014).

69. Grusch M. *et al.* Spatio-temporally precise activation of engineered receptor tyrosine kinases by light. *The EMBO Journal* **33**, 1713–1726 (2014).

70. Bugaj L. J. *et al.* Regulation of endogenous transmembrane receptors through optogenetic Cry2 clustering. *Nat. Commun.* **6**, ncomms7898 (2015).

71. Ingles-Prieto A. *et al.* Light-assisted small-molecule screening against protein kinases. *Nat. Chem. Biol.* **11**, 952–954 (2015).

72. Fortunato A. E., Annunziata R., Jaubert M., Bouly J.-P., Falciatore A. Dealing with light: The widespread and multitasking cryptochrome/photolyase family in photosynthetic organisms. *J. Plant Physiol.* **172**, 42–54 (2015).

73. Kennedy M. J. *et al.* Rapid blue-light-mediated induction of protein interactions in living cells. *Nat. Methods* **7**, 973–975 (2010).

74. Idevall-Hagren O., Dickson E. J., Hille B., Toomre D. K., De Camilli P. Optogenetic control of phosphoinositide metabolism. *Proc. Natl. Acad. Sci. U. S. A.* **109**, 13894–13895 (2012).

75. Konermann S. *et al.* Optical control of mammalian endogenous transcription and epigenetic states. *Nature*, nature12466 (2013).

76. Lee S. *et al.* Reversible protein inactivation by optogenetic trapping in cells. *Nat. Methods* **11**, 633–636 (2014).

77. Conrad K. S., Manahan C. C., Crane B. R. Photochemistry of flavoprotein light sensors. *Nat. Chem. Biol.* **10**, 801–809 (2014).

78. Liu H., Liu B., Zhao C., Pepper M., Lin C. The action mechanisms of plant cryptochromes. *Trends in Plant Science* **16**, 684–691 (2011).

79. Canamero R. *et al.* Cryptochrome photoreceptors cry1 and cry2 antagonistically regulate primary root elongation in *Arabidopsis thaliana*. *Planta* **224**, 995–1003 (2006).

80. Ohgishi M., Saji K., Okada K., Sakai T. Functional analysis of each blue light receptor, cry1, cry2, phot1, and phot2, by using combinatorial multiple mutants in *Arabidopsis*. *Proc. Natl. Acad. Sci. U. S. A.* **101**, 2223–2228 (2004).

81. Stein E., Zou Y., Poo M.-m., Tessier-Lavigne M. Binding of DCC by netrin-1 to mediate axon guidance independent of Adenosine A2B receptor activation. *Science* **291**, 1976–1982 (2001).

82. Brenner S. The genetics of *Caenorhabditis elegans*. *Genetics* **77**, 71–94 (1974).

83. Mello C., Fire A. DNA transformation. *Methods Cell Biol.* **48**, 451–482 (1995).

84. Matsuki M., Kunitomo H., Iino Y. Goα regulates olfactory adaptation by antagonizing Gqα-DAG signaling in *Caenorhabditis elegans*. *Proc. Natl. Acad. Sci. U. S. A.* **103**, 1112–1117 (2006).

85. Liu H. *et al.* Photoexcited CRY2 interacts with CIB1 to regulate transcription and floral initiation in *Arabidopsis*. *Science* **322**, 1535–1539 (2008).

86. Gomez T. M., Robles E., Poo M.-m., Spitzer N. C. Filopodial calcium transients promote substrate-dependent growth cone turning. *Science* **291**, 1983–1987 (2001).

87. Guirland C., Buck K. B., Gibney J. A., DiCicco-Bloom E., Zheng J. Q. Direct cAMP signaling through G-protein-coupled receptors mediates growth cone attraction induced by pituitary adenylate cyclase-activating polypeptide. *J. Neurosci.* **23**, 2274–2283 (2003).

88. McIntire S. L., Reimer R. J., Schuske K., Edwards R. H., Jorgensen E. M. Identification and characterization of the vesicular GABA transporter. *Nature* **389**, 870–876 (1997).

89. Yu X. *et al.* Formation of nuclear bodies of *Arabidopsis* CRY2 in response to blue light is associated with its blue light–dependent degradation. *The Plant Cell Online* **21**, 118–130 (2009).

90. Yu X. *et al.* Derepression of the NC80 motif is critical for the photoactivation of *Arabidopsis* CRY2. *Proc. Natl. Acad. Sci. U. S. A.* **104**, 7289–7294 (2007).

91. Shekarabi M., Kennedy T. E. The netrin-1 receptor DCC promotes filopodia formation and cell spreading by activating Cdc42 and Rac1. *Mol. Cell. Neurosci.* **19**, 1–17 (2002).

92. Che D. L., Duan L., Zhang K., Cui B. The dual characteristics of light-induced cryptochrome 2 homo-oligomerization and hetero-dimerization for optogenetic manipulation in mammalian cells. *ACS Synthetic Biology*, acssynbio.5b00048 (2015).

93. Culotti J. G., Merz D. C. DCC and netrins. *Curr. Opin. Cell Biol.* **10**, 609–613 (1998).

94. Ren X.-r. *et al.* Focal adhesion kinase in netrin-1 signaling. *Nat. Neurosci.* **7**, 1204–1212 (2004).

95. Xie Y. *et al.* Phosphatidylinositol transfer protein-α in netrin-1-induced PLC signalling and neurite outgrowth. *Nat. Cell Biol.* **7**, 1124–1132 (2005).

96. Hallett R., Zimmerman S. P., Yumerefendi H., Bear J. E., Kuhlman B. Correlating *in vitro* and *in vivo* activities of light inducible dimers: A cellular optogenetics guide. *ACS Synthetic Biology*, acssynbio.5b00119 (2015).

97. Black B. J., Gu L., Mohanty S. K. Highly effective photonic cue for repulsive axonal guidance. *PLoS One* **9**, e86292 (2014).

98. Huber A. B., Kolodkin A. L., Ginty D. D., Cloutier J.-F. Signaling at the growth cone: Ligand–receptor complexes and the control of axon growth and guidance. *Annu. Rev. Neurosci.* **26**, 509–563 (2003).

99. Keleman K., Dickson B. J. Short- and long-range repulsion by the *Drosophila* Unc5 netrin receptor. *Neuron* **32**, 605–617 (2001).

100. Byerly L., Cassada R. C., Russell R. L. The life cycle of the nematode *Caenorhabditis elegans*: I. Wild-type growth and reproduction. *Dev. Biol.* **51**, 23–33 (1976).

101. Consortium T. C. e. S. Genome sequence of the nematode *C. elegans*: A platform for investigating biology. *Science* **282**, 2012–2018 (1998).

102. Ward S., Thomson N., White J. G., Brenner S. Electron microscopical reconstruction of the anterior sensory anatomy of the nematode *Caenorhabditis elegans*. *The Journal of Comparative Neurology* **160**, 313–337 (1975).

103. Stinchcomb D. T., Shaw J. E., Carr S. H., Hirsh D. Extrachromosomal DNA transformation of *Caenorhabditis elegans*. *Mol. Cell. Biol.* **5**, 3484–3496 (1985).

104. Wadsworth W. G. Moving around in a worm: Netrin UNC-6 and circumferential axon guidance in *C. elegans*. *Trends Neurosci.* **25**, 423–429 (2002).

105. Gitai Z., Yu T. W., Lundquist E. A., Tessier-Lavigne M., Bargmann C. I. The netrin receptor UNC-40/DCC stimulates axon attraction and outgrowth through enabled and, in parallel, rac and unc-115/ablim. *Neuron* **37**, 53–65 (2003).

106. Norris A. D., Lundquist E. A. UNC-6/netrin and its receptors UNC-5 and UNC-40/DCC modulate growth cone protrusion *in vivo* in *C. elegans*. *Development* **138**, 4433–4442 (2011).

107. Adler C. E., Fetter R. D., Bargmann C. I. UNC-6/netrin induces neuronal asymmetry and defines the site of axon formation. *Nat. Neurosci.* **9**, 511–518 (2006).

108. White J. G., Southgate E., Thomson J. N., Brenner S. The structure of the nervous system of the nematode *Caenorhabditis elegans*. *Philosophical Transactions of the Royal Society of London B: Biological Sciences* **314**, 1–340 (1986).

109. Nagel G. *et al.* Light activation of Channelrhodopsin-2 in excitable cells of *Caenorhabditis elegans* triggers rapid behavioral responses. *Curr. Biol.* **15**, 2279–2284 (2005).

110. Hedgecock E. M., Culotti J. G., Hall D. H. The *unc-5*, *unc-6*, and *unc-40* genes guide circumferential migrations of pioneer axons and mesodermal cells on the epidermis in *C. elegans*. *Neuron* **4**, 61–85 (1990).

111. Chan S. S. Y. *et al.* UNC-40, a *C. elegans* homolog of DCC (Deleted in Colorectal Cancer), is required in motile cells responding to UNC-6 netrin cues. *Cell* **87**, 187–195 (1996).

112. Wong M.-C., Martynovsky M., Schwarzbauer J. E. Analysis of cell migration using *Caenorhabditis elegans* as a model system. *Methods Mol. Biol.* **769**, 233–247 (2011).

113. Lewis J. A., Wu C. H., Levine J. H., Berg H. Levamisole-resistant mutants of the nematode *C. elegans* appear to lack pharmacological acetylcholine receptors. *Neuroscience* **5**, 967–989 (1980).

114. Norris A. D., Sundararajan L., Morgan D. E., Roberts Z. J., Lundquist E. A. The UNC-6/netrin receptors UNC-40/DCC and UNC-5 inhibit growth cone filopodial protrusion via UNC-73/Trio, Rac-like GTPases and UNC-33/CRMP. *Development* **141**, 4395–4405 (2014).